

This is an Accepted Manuscript of an article published by Taylor & Francis in *Alcheringa: An Australasian Journal of Palaeontology* on 7 May 2019, available online:

<https://doi.org/10.1080/03115518.2019.1594380>.

The full details of the published version of the article are as follows:

TITLE: The architecture of cancellous bone in the hindlimb of moa (Aves: Dinornithiformes), with implications for stance and gait

AUTHORS: Peter J. Bishop, R. Paul Scofield & Scott A. Hocknull

JOURNAL TITLE: *Alcheringa: An Australasian Journal of Palaeontology*

PUBLISHER: Taylor & Francis

PUBLICATION DATE: 7 May 2019 (online)

DOI: 10.1080/03115518.2019.1594380

1 The architecture of cancellous bone in the hindlimb of moa  
2 (Aves: Dinornithiformes), with implications for stance and gait

3  
4 P.J. BISHOP, R.P. SCOFIELD and S.A. HOCKNULL.

5  
6 BISHOP, P.J., SCOFIELD, R.P. & HOCKNULL, S.A. 201X. The architecture of cancellous bone  
7 in the hindlimb of moa (Aves: Dinornithiformes), with implications for stance and gait.  
8 *Alcheringa* XXX, X–X. ISSN 0311-5518.

9  
10 The extinct, flightless moa of New Zealand included some of the largest birds to have existed, and possessed  
11 many distinguishing pelvic and hindlimb osteological features. These features may have influenced stance and  
12 gait in moa compared to extant birds. One means of assessing locomotor biomechanics, particularly for extinct  
13 species, is quantitative analysis of the architecture of cancellous bone, since this architecture is adapted to suit  
14 its mechanical environment with high sensitivity. This study investigated the three-dimensional architecture of  
15 cancellous bone in the femur, tibiotarsus and fibula of three moa species: *Dinornis robustus*, *Pachyornis*  
16 *elephantopus* and *Megalapteryx didinus*. Using computed tomographic X-ray scanning and previously  
17 developed fabric analysis techniques, the spatial variation in cancellous bone fabric patterns in moa was found  
18 to be largely comparable to that previously reported for extant birds, particularly large species. Moa hence  
19 likely used postures and kinematics similar to those employed by large extant bird species, but this  
20 interpretation is tentative on account of relatively small sample sizes. A point of major difference between moa  
21 and extant birds concerns the diaphyses; cancellous bone invades the medullary cavity in both groups, but the  
22 invasion is far more extensive in moa. Combined with previous assessments of cortical geometry, this further  
23 paints a picture of at least some moa species possessing very robust limb bones, for which a convincing  
24 explanation remains to be determined.

1  
2  
3  
4  
5  
6  
7  
8  
9  
10  
11  
12  
13  
14  
15  
16  
17  
18  
19  
20  
21  
22  
23  
24  
25  
26  
27  
28  
29  
30  
31  
32  
33  
34  
35  
36  
37  
38  
39  
40  
41  
42  
43  
44  
45  
46  
47  
48  
49  
50  
51  
52  
53  
54  
55  
56  
57  
58  
59  
60

28 P.J. Bishop\* [pbishop@rvc.ac.uk], Structure and Motion Laboratory, Department of Comparative Biomedical  
29 Sciences, Royal Veterinary College, Hawkshead Lane, Hatfield, Hertfordshire AL9 7TA, United Kingdom; R.P.  
30 Scofield† [pscofield@canterburymuseum.com], Canterbury Museum, Rolleston Avenue, Christchurch 8013,  
31 New Zealand; S.A. Hocknull‡ [scott.hocknull@qm.qld.gov.au], Geosciences Program, Queensland Museum,  
32 122 Gerler Road, Hendra, Queensland 4011, Australia. \*Also affiliated with: Geosciences Program,  
33 Queensland Museum, 122 Gerler Road, Hendra, Queensland 4011, Australia. †Also affiliated with:  
34 Department of Geological Sciences, University of Canterbury, Christchurch 8140, New Zealand. ‡Also  
35 affiliated with: School of Biosciences, University of Melbourne, Royal Parade, Parkville, Victoria 3052,  
36 Australia.

38 Key words: moa, cancellous bone, hindlimb, locomotion, biomechanics.

40 Running head: moa cancellous bone structure

1  
2  
3 55 BECOMING extinct only relatively recently, the flightless moa (Aves: Palaeognathae:  
4  
5 56 Dinornithiformes) of New Zealand included some of the largest birds to have ever existed.  
6  
7  
8 57 Across the nine currently recognized species (Worthy & Scofield 2012), body mass in moa  
9  
10 58 has been estimated to range from about 20 kg in *Megalapteryx didinus* Owen, 1883 to over a  
11  
12 59 quarter of a tonne in *Dinornis robustus* Owen, 1846 (Alexander 1983a, Anderson 1989,  
13  
14 60 Worthy & Holdaway, 2002, Murray & Vickers-Rich 2004, Brassey et al. 2013). Moa also  
15  
16 61 possessed a number of unique anatomical features of the pelvis and femur (Worthy &  
17  
18 62 Holdaway 2002), as well as unusually proportioned hindlimb bones, in terms of both  
19  
20 63 intersegmental proportions (Gatesy & Middleton, 1997) and whole-bone robusticity  
21  
22 64 (Alexander 1983a, Alexander 1983b, Doube et al. 2012, Brassey et al. 2013). Collectively,  
23  
24 65 these observations suggest that moa, particularly the larger species, may have stood and  
25  
26 66 moved in a manner different to extant birds.

27  
28  
29  
30  
31 67 Moa were unique among birds in completely lacking wings, with the fused  
32  
33 68 scapulocoracoid lacking even a glenoid (Worthy & Holdaway 2002, Worthy & Scofield  
34  
35 69 2012). They also possessed an acarinate sternum, and the pelvis of all species except  
36  
37 70 *Megalapteryx didinus* and *Anomalopteryx didiformis* (Owen, 1844) was very broad caudal  
38  
39 71 to the acetabulum. These features suggest that the whole-body centre of mass of moa may  
40  
41 72 have been more caudally positioned compared to extant birds, which would have hence  
42  
43 73 influenced hindlimb positioning, stance and gait (Alexander 1983a). Despite these oddities,  
44  
45 74 the articular surface morphology of the main bones of the moa hindlimb does not differ  
46  
47 75 appreciably from that of extant birds, implying minimal differences in limb articulation, and  
48  
49 76 therefore posture (Anderson 1989, Worthy & Holdaway 2002, Zinoviev 2013). The  
50  
51 77 hindlimb myology of moa is also inferred to be largely comparable to that of extant  
52  
53 78 palaeognathous birds, with few major differences (Bishop 2015), also suggestive of minimal  
54  
55 79 difference in locomotor behaviour compared to extant birds. A number of fossil moa  
56  
57  
58  
59  
60

1  
2  
3 80 trackways (sequences of footprints) are known, but analyses to date suggest that these too  
4  
5 81 are comparable to those made by extant birds (Worthy & Holdaway 2002); in any case, they  
6  
7 82 do not reveal any insight to movements of more proximal limb segments (Thulborn 1990,  
8  
9 83 Hutchinson & Gatesy 2006).

10  
11  
12 84 To better clarify stance and gait in moa, and to resolve apparently conflicting lines of  
13  
14 85 evidence, one way forward is to study evidence of locomotor biomechanics recorded in limb  
15  
16 86 bone osteology. The spatial distribution of cortical bone at midshaft has been examined  
17  
18 87 previously (Alexander 1983b, Worthy 1989, Brassey et al. 2013), but inferences drawn from  
19  
20 88 such observations must be viewed with caution, since experimental evidence with modern  
21  
22 89 species indicates that cortical bone morphology does not always correlate with the nature of  
23  
24 90 bone loading (e.g., Thomason 1995, Demes et al. 2001, Demes et al. 1998, Main &  
25  
26 91 Biewener 2004, Pearson & Lieberman 2004, Lieberman et al. 2004, Demes 2007, Wallace et  
27  
28 92 al. 2014). In contrast, the architecture of cancellous bone ('spongy bone') does show a  
29  
30 93 strong correlation with loading conditions experienced in vivo (Kivell 2016). Cancellous  
31  
32 94 bone is sensitive to its mechanical environment, and is able to adapt its architecture to suit  
33  
34 95 this environment in a highly predictable fashion. For example, numerous studies have  
35  
36 96 demonstrated that increased loading magnitude leads to an increase in the volume fraction  
37  
38 97 occupied by bone material (Biewener et al. 1996, van der Meulen et al. 2006, Wang et al.  
39  
40 98 2012), whereas a change in loading direction leads to a reorientation of the dominant  
41  
42 99 direction of the comprising trabeculae (Radin et al. 1982, Goldstein et al. 1991, Mullender  
43  
44 100 & Huiskes 1995, Huiskes et al. 2000, Adachi et al. 2001, Ruimerman et al. 2005, Pontzer et  
45  
46 101 al. 2006, Polk et al. 2008, Volpato et al. 2008, Barak et al. 2011). The mechanobiological  
47  
48 102 processes underpinning these responses are likely founded upon achieving a uniform  
49  
50 103 distribution of bone tissue strain, averaged across time and loading conditions (Fyhrie &  
51  
52 104 Carter 1986, Boyle & Kim 2011, Christen et al. 2013).

1  
2  
3 105 Given how well cancellous bone adapts to its mechanical environment, it is of little  
4  
5 106 surprise that differences in locomotor behaviour among extant species are often manifest in  
6  
7 107 differences in cancellous bone architecture (Fajardo & Müller 2001, Ryan & Ketcham  
8  
9 108 2002b, 2005, Maga et al. 2006, Hébert et al. 2012, Ryan & Shaw 2012, Barak et al. 2013,  
10  
11 109 Su et al. 2013, Tsegai et al. 2013, Matarazzo 2015, Kivell 2016, Georgiou et al. 2018). Of  
12  
13 110 particular note is that the principal orientations of trabeculae (i.e. the cancellous bone fabric)  
14  
15 111 tends to be especially telling of differences in locomotor behaviour (Ryan & Ketcham  
16  
17 112 2002b, 2005, Maga et al. 2006, Hébert et al. 2012, Ryan & Shaw 2012, Barak et al. 2013,  
18  
19 113 Su et al. 2013, Tsegai et al. 2013, Matarazzo 2015, Amson et al. 2017, Bishop et al. 2018b).  
20  
21 114 The architecture of cancellous bone therefore has the potential to shed new insight on whole-  
22  
23 115 bone loading mechanics and locomotor behaviour in extinct species such as moa (Bishop et  
24  
25 116 al. 2018b).

26  
27  
28  
29  
30 117 Cancellous bone architecture has recently been surveyed in the main limb bones of a  
31  
32 118 wide variety of extant ground-dwelling bird species (Bishop et al. 2018b). That study  
33  
34 119 identified patterns of fabric directionality which correlate to size-related changes in hip and  
35  
36 120 knee flexion during avian stance or gait, as well as a ubiquity of oblique trabeculae in the  
37  
38 121 femoral and tibial diaphyses that corresponds to strong torsional loading of these bones  
39  
40 122 during locomotion. These results provide a comparative framework upon which cancellous  
41  
42 123 bone architecture in moa hindlimb bones may be investigated, insofar as it relates to limb  
43  
44 124 bone loading and locomotor biomechanics. The present study aimed to investigate the three-  
45  
46 125 dimensional (3-D) architecture of cancellous bone in the hindlimb of three moa species,  
47  
48 126 *Dinornis robustus*, *Pachyornis elephantopus* (Owen, 1858) and *Megalapteryx didinus*. The  
49  
50 127 results of quantitative and qualitative analyses, when compared to similar results obtained  
51  
52 128 for extant birds, can help resolve questions concerning stance and gait in these species.  
53  
54 129 Given the size-related trends in posture and cancellous bone architecture reported previously  
55  
56  
57  
58  
59  
60

1  
2  
3 130 for extant birds by Bishop et al. (2018a,b), it is predicted that moa will exhibit architectural  
4  
5 131 patterns most comparable to large extant birds. In addition to providing insight into moa  
6  
7 132 locomotor biomechanics specifically, the results of this study can more broadly also shed  
8  
9 133 new light on the potential consequences of large body size for avian bipedalism.  
10  
11  
12  
13  
14

134

## 15 135 Material and methods

16  
17 136 The methodology employed in this study followed that outlined previously by Bishop et al.  
18  
19 137 (2018b), and so only a brief overview is given here. The species examined were chosen so as  
20  
21 138 to sample all three moa families as well as varying body sizes and proportions: the  
22  
23 139 dinornithid *Dinornis robustus* is large (up to 250 kg) and tall, the emeid *Pachyornis*  
24  
25 140 elephantopus is medium-sized (around 100 kg) and very graviportal, and the megalapterygid  
26  
27 141 *Megalapteryx didinus* is small (around 20 kg) and relatively gracile. The present study  
28  
29 142 focused on three main bones of the moa hindlimb, the femur, tibiotarsus and fibula; these  
30  
31 143 were the bones studied previously in extant birds, and collectively give a full picture of the  
32  
33 144 hip and knee joints. All specimens were obtained from the Natural History Collections of the  
34  
35 145 Canterbury Museum (Table 1); the large sizes of the specimens studied indicate that they  
36  
37 146 were from adult birds. The 3-D architecture of cancellous bone in the fossil specimens was  
38  
39 147 acquired through X-ray computed tomographic (CT) scanning, using a Siemens Somatom  
40  
41 148 Definition Flash dual energy scanner (Siemens AG, Germany); the scan settings used are  
42  
43 149 listed in Table 1. The resulting scans were processed using the software ImageJ 1.47  
44  
45 150 (<http://imagej.nih.gov/ij/>) and Mimics 17.0 (Materialize NV, Belgium), following protocol 2  
46  
47 151 of Bishop et al. (2018b). This was possible because of the excellent preservation of the  
48  
49 152 specimens, with little (if any) matrix inside the bones, affording good contrast between bone  
50  
51 153 and non-bone phases in the CT scans.  
52  
53  
54  
55  
56  
57  
58  
59 154  
60

1  
2  
3 155 The processed and segmented CT scans were then subject to a number of architectural  
4  
5 156 analyses. The first was an analysis of cancellous bone fabric, where the 3-D fabric tensor  
6  
7  
8 157 (Cowin, 1986) was calculated using the star volume distribution method (Cruz-Orive et al.  
9  
10 158 1992, Odgaard 1997, 2001), as implemented in the software Quant3D 2.3 (Ryan & Ketcham  
11  
12 159 2002a,b, Ketcham & Ryan 2004). When conducted for numerous volumes of interest  
13  
14 160 throughout a whole bone, this provides an assessment of how fabric direction (essentially,  
15  
16 161 trabecular orientation) varies spatially across the bone. In some specimens over 850  
17  
18 162 individual volumes of interest were analysed for a given bone. The second analysis  
19  
20 163 conducted concerned the results for the femoral head and medial femoral condyle, in  
21  
22 164 particular, the orientation of the primary fabric direction (the direction of strongest  
23  
24 165 trabecular alignment, equivalent to the first eigenvector of the fabric tensor) in these regions  
25  
26 166 of the bone. Here, the mean orientation of the primary fabric direction across each  
27  
28 167 anatomical region was calculated and referenced to an explicit femoral anatomical  
29  
30 168 coordinate system. Previously, these mean orientations were found to correlate with the  
31  
32 169 degree of hip and knee flexion in extant bipeds (Bishop et al. 2018b), and may therefore  
33  
34 170 provide insight into posture in extinct moa. These mean orientations, in terms of their  
35  
36 171 sagittal components, were also compared to body size, where the interarticular length of the  
37  
38 172 femur (i.e., less the trochanteric crest) was taken as a proxy for body size  
39  
40  
41  
42  
43  
44

45 173 The third and final analysis involved examination of gross morphological characteristics  
46  
47 174 of cancellous bone architecture in the diaphysis (shaft) of the femur and tibiotarsus. This  
48  
49 175 was undertaken through a categorical scoring study performed by five independent,  
50  
51 176 volunteer observers; these volunteers were the same as those used in the study of extant bird  
52  
53 177 bones (Bishop et al. 2018b), and were blind to the objectives of the current study. Using 3-D  
54  
55 178 isosurface renderings derived from the segmented CT scans, three features were scored: the  
56  
57 179 bulk spatial extent of cancellous bone in the diaphysis, the tendency of trabeculae to be  
58  
59  
60

1  
2  
3 180 closely associated with other trabeculae, and the average orientation of trabeculae with  
4  
5 181 respect to the long-axis of the bone. Following scoring, the mean score across the five  
6  
7 182 observers was taken for each bone and for each morphological feature. The actual  
8  
9 183 architecture of cancellous bone in the diaphyses was also assessed by the authors through  
10  
11 184 visualization of the isosurface renderings.  
12  
13  
14

15 185 Statistical comparison between moa and extant birds was conducted for the calculated  
16  
17 186 mean primary fabric directions for the femoral head and medial femoral condyle in both  
18  
19 187 groups. Setting an a priori significance level of  $p = 0.05$ , the 95% confidence interval of the  
20  
21 188 mean direction ('confidence cone') for both groups was then calculated using the software  
22  
23 189 StereoNet 9.5 (Allmendinger et al. 2013, Cardozo & Allmendinger 2013). If overlap  
24  
25 190 occurred between the mean direction of one group and the 95% confidence cone of the other  
26  
27 191 group, the mean directions of the two groups were not statistically significantly different; if  
28  
29 192 no overlap occurred between a mean direction of one group and the confidence cone of the  
30  
31 193 other group, the means were different (Butler 1992, Ryan & Ketcham 2005, Allmendinger et  
32  
33 194 al. 2013.). However, if there was overlap between the confidence cones of both groups, but  
34  
35 195 not between mean directions and confidence cones, an F-test was used to determine if the  
36  
37 196 difference in means was due to sampling error (i.e., inadequate sample size), rather than  
38  
39 197 legitimate differences between groups (Butler, 1992). In addition, comparisons of mean  
40  
41 198 orientation to body size were assessed using major axis regression in PAST 3.09 (Hammer  
42  
43 199 et al. 2001), with significance values calculated using a 100,000-replicate permutation test  
44  
45 200 of the slope (Legendre & Legendre 2012), as done previously.  
46  
47  
48  
49

50  
51 201 The results of the categorical scoring analyses were also compared to body size, where  
52  
53 202 the interarticular length of the relevant bone was taken as a proxy for body size, and  
54  
55 203 compared to the patterns observed for extant birds by Bishop et al. (2018b). Comparisons  
56  
57 204 used major axis regression as implemented above. The reliability of the scorers in the  
58  
59  
60

1  
2  
3 205 analysis of diaphyseal cancellous bone was previously assessed (Bishop et al. 2018b), and  
4  
5 206 found to be moderate to good across the three features examined. Nevertheless, the results  
6  
7 207 presented here should still be viewed tentatively, pending the assessments being undertaken  
8  
9  
10 208 by a greater number of scorers for more specimens.

11  
12 209

## 15 210 Results

### 17 211 Summary

19 212 A brief overview of the key observations are first presented here, before being presented in  
20  
21  
22 213 full for each bone. The femur of each species displays architectural patterns broadly  
23  
24 214 comparable to that observed in extant birds, particularly larger species, including in regards  
25  
26 215 to relatively limited anterior and posterior inclination of the primary fabric direction in the  
27  
28 216 head and medial condyle, respectively. The very broad distal femora of *D. robustus* and *P.*  
29  
30 217 *elephantopus* are associated with a radiating pattern in the coronal plane, which is not  
31  
32  
33 218 known in extant birds of any size. Cancellous bone architecture in the tibiotarsus and fibula  
34  
35 219 of moa shows strong resemblance to that observed in extant birds, including a highly  
36  
37 220 anisotropic pattern in the distal tibiotarsus. As with extant birds, the femoral and tibial  
38  
39 221 diaphyses of moa possess abundant and markedly oblique trabeculae, although in moa the  
40  
41 222 abundance is conspicuously greater.

42  
43  
44 223 On a nomenclatural note, the term ‘proximodistal’ is always used here in reference to the  
45  
46 224 proximodistal axis of the whole bone under consideration, regardless of the specific  
47  
48 225 anatomical region concerned.

49  
50 226

### 54 227 Femur

56 228 Cancellous bone architecture in the moa proximal femur displays a pattern of spatial  
57  
58 229 variation in fabric directions which is quite comparable to that previously reported for extant

1  
2  
3 230 birds (Bishop et al. 2018b). None of the bones studied were invaded by pneumatopores to  
4  
5 231 any significant extent, and thus the influence that pneumatization may have on cancellous  
6  
7  
8 232 bone architecture in extant birds (Bishop et al. 2018b) was not of concern here. The primary  
9  
10 233 fabric direction ( $u_1$ ) in the femoral head and neck is oriented largely proximodistally, with a  
11  
12 234 variable amount of anteromedial inclination (Fig. 1A, B). Under the facies antitrochanterica,  
13  
14  
15 235 the anterior inclination diminishes while the medial inclination can become stronger or  
16  
17 236 weaker (Fig. 1C, D); sometimes a slight lateral inclination is also possible. The same general  
18  
19 237 pattern continues anteriorly toward the trochanteric crest, although it tends to be less  
20  
21  
22 238 strongly organized in *M. didinus* compared to *D. robustus* (Fig. 1E, F); also, in *D. robustus*,  
23  
24 239  $u_1$  takes on a gentle anterior inclination once again (Fig. 1G, H).

25  
26 240 [Fig. 1]  
27  
28  
29 241

30  
31 242 In the distal femur,  $u_1$  is also oriented in a mostly proximodistal fashion. A double-  
32  
33 243 arcuate pattern, parallel to the sagittal plane, was noted previously for the central metaphysis  
34  
35 244 of large extant species of birds (Bishop et al. 2018b), but this is not particularly well-  
36  
37  
38 245 developed in moa (Fig. 2A). Indeed, such a pattern is veritably absent in *M. didinus*. On the  
39  
40 246 other hand, a well-developed ‘radiating’ pattern is evident in the coronal plane in *D.*  
41  
42 247 *robustus* and *P. elephantopus*, whereby the orientation of  $u_1$  is directed towards the medial  
43  
44 248 condyle medially and directed towards the lateral condyle laterally, sweeping across the  
45  
46  
47 249 metaphysis (Fig. 2B). This pattern is not well developed in extant birds; its occurrence in *D.*  
48  
49 250 *robustus* and *P. elephantopus* may reflect the great mediolateral breadth of the distal end of  
50  
51 251 the femur relative to the shaft, flaring out to the sides more. The architectural patterns in the  
52  
53 252 medial and lateral condyles are more comparable to the pattern in extant birds (Fig. 2C–F).  
54  
55  
56 253 Within both condyles, the orientation of  $u_1$  is largely subparallel to the sagittal plane, and it  
57  
58 254 usually has a marked posterior inclination, particularly in the medial condyle. As with large  
59  
60

1  
2  
3 255 extant birds (Bishop et al. 2018b),  $u_1$  sweeps a wide arc in the sagittal plane (usually well in  
4  
5 256 excess of  $100^\circ$ ), such that in the posterior extremities of the condyles, it can be  
6  
7  
8 257 perpendicular to the proximodistal axis of the bone. Moreover, in the anterior parts of the  
9  
10 258 condyles,  $u_1$  is often anterodistally directed. As observed previously for extant birds, as well  
11  
12 259 as humans and extinct, non-avian theropod dinosaurs (Bishop et al. 2018b), the secondary  
13  
14 260 fabric direction ( $u_2$ ) forms a ‘butterfly pattern’ in the plane that passes through the centres of  
15  
16 261 both condyles (Fig. 2G). Here, two ‘tracts’ (one in each condyle) arc from the anterior aspect  
17  
18 262 of their respective condyle back towards the posterior aspect.  
19  
20

21 [Fig. 2]  
22  
23  
24 264

25  
26 265 In large extant birds, it was previously observed that a transect through the metaphysis  
27  
28 266 from the ends of the femur towards the diaphysis often saw a noticeable increase in the  
29  
30 267 ‘disorganization’ of the orientations of  $u_1$ . That is, the vectors took on a more oblique  
31  
32 268 orientation and the change in direction across the bone was no longer gradual (Bishop et al.  
33  
34 269 2018b). Such a change was apparent in both ends of the femora of *M. didinus*, as well as the  
35  
36 270 proximal femur of *D. robustus* and *P. elephantopus* (Fig. 3), but it was not particularly  
37  
38 271 evident in the distal femur of the latter two species. This may be in part due to the obliquity  
39  
40 272 already present in the distal femur of *D. robustus* and *P. elephantopus*, resulting from the  
41  
42 273 ‘radiating’ pattern in the coronal plane noted above.  
43  
44  
45  
46

47 [Fig. 3]  
48

49 275 Results of the calculations of mean primary fabric direction are presented in Fig. 4.  
50  
51 276 Consistent with the qualitative observations noted above, the mean orientation of  $u_1$  in the  
52  
53 277 femoral head is anteromedially directed (moving proximally) for all six moa specimens (Fig.  
54  
55 278 4A). This direction is similar to the general pattern observed for extant birds. Indeed, the  
56  
57 279 mean direction of both groups falls within the 95% confidence cone of the mean of the other  
58  
59  
60

1  
2  
3 280 group, indicating no significant difference between group means ( $p > 0.05$ ). The mean  
4  
5 281 orientation of  $u_1$  in the medial femoral condyle is posteriorly directed (moving distally) for  
6  
7 282 all six moa specimens (Fig. 4A), although some had a slight medial inclination whereas  
8  
9 283 others had a slight lateral inclination. Unlike the femoral head, the mean direction across  
10  
11 284 moa as a whole is different from the mean direction of extant birds as a whole ( $p < 0.05$ ; Fig.  
12  
13 285 4A), but it cannot be discounted that this difference was due to inadequate sampling of the  
14  
15 286 underlying populations ( $F_{2,52} = 1.819$ ,  $p = 0.172$ ). In terms of the amount of sagittal  
16  
17 287 inclination of  $u_1$  with respect to femoral length, moa are seen to follow and reinforce the  
18  
19 288 patterns observed in extant birds. Previously, the amount of anterior inclination of  $u_1$  in the  
20  
21 289 femoral head of extant birds was not able to be demonstrated to correlate significantly with  
22  
23 290 femur length (Bishop et al. 2018b). However, the inclusion of data from the moa specimens  
24  
25 291 examined here produces a statistically significant relationship, with larger birds tending to  
26  
27 292 exhibit lower anterior inclination ( $p = 0.01687$ ; Fig. 4B). In a similar fashion to the femoral  
28  
29 293 head, the inclusion of data for the medial femoral condyle of moa reinforces the tendency for  
30  
31 294 larger birds to exhibit a lower degree of posterior inclination of  $u_1$  in this region of the femur  
32  
33 295 ( $p = 0.00062$ ; Fig. 4C).

34  
35  
36  
37  
38  
39  
40 [Fig. 4]

41  
42 297  
43  
44 298 Tibiotarsus

45  
46  
47 299 As with the femur, the spatial pattern of cancellous bone fabric in the tibiotarsus of moa is  
48  
49 300 quite comparable to that previously reported for extant birds (Bishop et al. 2018b). The  
50  
51 301 orientation of  $u_1$  in the proximal tibia is overall proximodistal, but superimposed upon this  
52  
53 302 are marked inclinations that vary throughout the bone. It has an anteroproximal inclination  
54  
55 303 in the cnemial crests, essentially following the anterior margins of the crests (Fig. 5A, B),  
56  
57 304 whereas under the condyles it has a marked posterior inclination, projecting up to  $30^\circ$   
58  
59  
60

1  
2  
3 305 posterior of the proximodistal axis (Fig. 5C–F). Additionally, under the lateral condyle,  
4  
5 306 there is also a strong lateral inclination (Fig. 5E), which as in extant birds can sometimes  
6  
7 307 exceed the amount of posterior inclination. Another feature often present in moa is a double-  
8  
9 308 arcuate pattern in  $u_1$  in the sagittal plane of the proximal metaphysis, whereby the individual  
10  
11 309 fabric vectors are largely contained within the sagittal plane. This feature was not always  
12  
13 310 present in extant birds (Bishop et al. 2018b), nor all moa specimens examined here, but is  
14  
15 311 well developed in *D. robustus* (Fig. 5G). Here, one tract arcs from the posterior metaphysis  
16  
17 312 anteriorly towards the cnemial crests, whereas the other arcs from the anterior metaphysis  
18  
19 313 posteriorly towards the articular condyles. A small quantity of cancellous bone is present  
20  
21 314 under the fibular crest of moa, but was usually not abundant enough to permit quantitative  
22  
23 315 fabric analysis. This is on account of both the relatively low projection of the crest from the  
24  
25 316 diaphysis in these species, and the fact that the crest comprised a large proportion of  
26  
27 317 relatively high-porosity cortical bone. Similar to the femur of moa, a transect through the  
28  
29 318 metaphysis from the proximal end of the tibia towards the diaphysis sometimes reveals  
30  
31 319 increased ‘disorganization’ of the orientations of  $u_1$  (Fig. 5H).

32  
33  
34  
35  
36  
37  
38 [Fig. 5]

39  
40 321 In the distal tibiotarsus, moa exhibit the same characteristic pattern previously reported  
41  
42 322 for birds (Bishop et al. 2018b). Here,  $u_1$  is largely oriented proximodistally and parallel to  
43  
44 323 the sagittal plane, whereas  $u_2$  is largely oriented anteroposteriorly and parallel to the sagittal  
45  
46 324 plane (Fig. 6A–E). Within the condyles themselves,  $u_1$  and  $u_2$  can become ‘rotated’ within  
47  
48 325 the sagittal plane to a variable degree. As in extant birds, this pattern reflects a highly  
49  
50 326 anisotropic arrangement of plate-like trabeculae, parallel to the sagittal plane, as is evident in  
51  
52 327 3-D renderings of the segmented CT scans (Fig. 6F). The ‘disorganization’ of  $u_1$  vectors  
53  
54 328 often observed for the femur and proximal tibiotarsus of moa (above) was not observed in  
55  
56 329 the distal tibiotarsus and any specimens examined.

1  
2  
3 330 [Fig. 6]  
4

5 331  
6

7  
8 332 Fibula  
9

10 333 Cancellous bone architecture in the moa fibula demonstrates the same spatial patterns as

11  
12 334 observed in extant birds (Bishop et al. 2018b). The orientation of  $u_1$  is consistent throughout

13  
14 335 the fibular head, being oriented proximodistally and subparallel to the local bone margin,

15  
16 336 with a gentle posterior inclination of up to  $20^\circ$  from the long-axis of the bone (Fig. 7). This

17  
18 337 posterior inclination tends to be greater in the more posterior parts of the fibular head. A

19  
20 338 small quantity of cancellous bone extends distally from the head, maintaining the same

21  
22 339 general fabric orientation as observed in the head. Some cancellous bone often occurs under

23  
24 340 the iliofibularis tubercle on the fibular shaft, but it was not extensive enough for quantitative

25  
26 341 analysis; rather, cortical thickness in this part of the bone is increased. Cancellous bone is

27  
28 342 virtually absent distal to the tubercle, where the bone rapidly diminishes to a thin splint of

29  
30 343 low-porosity cortical bone.  
31  
32

33 344 [Fig. 7]  
34

35 345  
36  
37

38 346 Diaphyses  
39

40 347 The results of the categorical analyses of diaphyseal cancellous bone architecture are

41  
42 348 presented in Fig. 8 and Table 2. As in large extant bird species, the femoral and tibial

43  
44 349 diaphyses of moa contain considerable quantities of cancellous bone, in which individual

45  
46 350 trabeculae are obliquely oriented relative to the bone long-axis, by about  $45^\circ$ . However, the

47  
48 351 patterns they exhibit are sometimes exaggerated compared to extant birds. The femoral

49  
50 352 diaphysis of all three moa species examined has a higher quantity of cancellous bone than

51  
52 353 would be predicted for their size, based on extant birds (higher 'extent scores', Fig. 8A); the

53  
54 354 data for moa consistently plot above the regression line derived previously for extant birds,  
55  
56  
57  
58  
59  
60

1  
2  
3 355 were it extrapolated to their size (dashed line in Fig. 8A). The same result occurs for the  
4  
5 356 tibial diaphysis in *D. robustus* and *P. elephantopus*, although the result is mixed for *M.*  
6  
7 357 *didinus* (Fig. 8B, dashed line). Trabeculae in the femoral diaphysis consequently tend to be  
8  
9 358 more strongly associated with each other: they are more closely packed together with high  
10  
11 359 ‘association scores’ (Fig. 8C). The pattern of association in the tibial diaphysis is more in  
12  
13 360 line with what would be expected based on extant birds (Fig. 8D). Similarly, the average  
14  
15 361 orientation of trabeculae in the femoral and tibial diaphyses is comparable to what would be  
16  
17 362 expected for birds of their size (comparable ‘orientation scores’, Fig. 8E,F), although it must  
18  
19 363 be acknowledged that the sample size for tibiae in extant birds was not large.  
20  
21  
22  
23

24 364 [Fig. 8]

25  
26 365 [Table 2]

27  
28 366 Three-dimensional visualization of the segmented CT scans further highlights the  
29  
30 367 aberrant nature of diaphyseal cancellous bone in moa in comparison to extant birds (Fig. 9,  
31  
32 368 Supplementary Movie S1). The medullary cavity is much reduced in volume, as a result of  
33  
34 369 extensive encroachment by cancellous bone into the diaphysis. Individual trabeculae can  
35  
36 370 also often be quite massive, being both long ( $> 20$  mm) and thick ( $> 1$  mm), and sometimes  
37  
38 371 plate-like as well. Despite this, moa display the same whole-bone gross architectural pattern  
39  
40 372 observed in the diaphyses of extant birds; in the femur especially, the typically oblique  
41  
42 373 trabeculae form conjugate helices that spiral about the length of the diaphysis. The condition  
43  
44 374 observed in moa may therefore be seen as quite similar to that of extant birds, just that it is  
45  
46 375 greatly exaggerated through a greater quantity of bone material per unit volume.  
47  
48  
49  
50

51 376 [Fig. 9]

52  
53 377

54  
55 378

56  
57  
58 379 Discussion  
59  
60

1  
2  
3 380 This study investigated the 3-D architecture of cancellous bone in the femur, tibiotarsus and  
4  
5 381 fibula of three species of moa, and comparisons were made to previously reported  
6  
7  
8 382 observations for these bones in a variety of extant species of ground-dwelling bird (Bishop  
9  
10 383 et al. 2018b). Overall, it was found that the spatial variation in cancellous bone fabric  
11  
12 384 patterns was quite comparable between moa and extant birds, for all three bones  
13  
14  
15 385 investigated. Where notable differences were found to exist between the two groups, these  
16  
17 386 can probably be attributed to either the unique osteology or generally large size of moa. For  
18  
19 387 example, the ‘radiating pattern’ of the primary fabric direction ( $u_1$ ) in the coronal plane of  
20  
21 388 the distal femur of *D. robustus* and *P. elephantopus* (Fig. 2B) is probably a consequence of  
22  
23 389 the strong mediolateral flaring of the distal end of the bone relative to the shaft in these large  
24  
25  
26 390 (and in the case of the latter, robust) species. Previously, it was shown that extant birds can  
27  
28 391 exhibit significant intra- and interspecific variation in cancellous bone architectural patterns  
29  
30 392 (Bishop et al. 2018b), and some results of the present study affirm this (Figs 4, 8). The  
31  
32 393 currently available sample sizes do not permit proper exploration of how such variation may  
33  
34 394 relate to differences in limb segment proportions, bone robusticity, ecology or other factors,  
35  
36 395 but this topic is well deserved of future study, and may provide further insight into moa  
37  
38 396 biology.

39  
40  
41  
42 397  
43  
44 398 That the fabric patterns of moa are qualitatively quite comparable to those reported for  
45  
46 399 extant birds, particularly large species, implies that moa limb bones experienced similar  
47  
48 400 loading regimes to those experienced by extant bird limb bones. This is further suggested by  
49  
50 401 the results of quantitative analysis of mean primary fabric directions in the femoral head and  
51  
52 402 medial femoral condyle (Fig. 4). Here, moa have clarified and reinforced the tendency for  
53  
54 403 larger birds to exhibit a lower degree of anterior inclination of the mean direction of  $u_1$  in  
55  
56 404 the femoral head, and a lower degree of posterior inclination of the mean direction of  $u_1$  in  
57  
58  
59  
60

1  
2  
3 405 the medial femoral condyle. This pattern parallels the tendency for larger birds to use a more  
4  
5 406 upright limb posture with more extended hip and knee joints, which likely causes  
6  
7 407 reorientation of joint contact forces to be more parallel to the long-axis of the femur (Bishop  
8  
9 408 et al. 2018a,b). In this regard, moa are simply following the same size-related biomechanical  
10  
11 409 trends observed in extant birds. The results therefore collectively suggest that moa used limb  
12  
13 410 postures and locomotor kinematics similar to those of large extant bird species, an  
14  
15 411 interpretation also suggested by bony articular surface morphology (Anderson 1989, Worthy  
16  
17 412 & Holdaway 2002, Zinoviev 2013). In light of the small sample sizes used for each species  
18  
19 413 and bone in the present study, this interpretation should be viewed as tentative, pending a  
20  
21 414 more comprehensive study that would facilitate more rigorous analysis. Nevertheless, if  
22  
23 415 locomotor biomechanics in moa did not appreciably differ from that of large extant birds,  
24  
25 416 this suggests that maximal locomotor performance – such as speed and agility capability –  
26  
27 417 of large moa species may have been relatively poorer compared to extant birds (but see  
28  
29 418 Hutchinson, 2004). This inference is based upon general principles derived from extant  
30  
31 419 terrestrial vertebrates: in the absence of major locomotor specialization or innovation,  
32  
33 420 relative locomotor performance declines with increasing body size (Garland 1983, Biewener  
34  
35 421 1989, Gatesy & Biewener 1991, Hutchinson et al. 2003, Sellers & Manning 2007, Clemente  
36  
37 422 et al. 2009, Dick & Clemente 2017).

38  
39 423  
40  
41 424 One striking difference between moa and extant birds that does not seem explicable by large  
42  
43 425 body size is the nature of cancellous bone in the femoral and tibial diaphyses. The medullary  
44  
45 426 cavity in both groups of bird is encroached by cancellous bone from the proximal and distal  
46  
47 427 ends of the bone, but it is generally much more ‘filled’ in moa compared to what would be  
48  
49 428 expected for their size (Figs 8, 9, Supplementary Movie S1). Additionally, individual  
50  
51 429 trabeculae in moa are often quite long and thick. This observation parallels those made for  
52  
53  
54  
55  
56  
57  
58  
59  
60

1  
2  
3 430 external diaphyseal (cortical) dimensions in moa limb bones: the diaphyses of moa,  
4  
5 431 particularly emeids (e.g., *P. elephantopus*), are more robust than what would be expected for  
6  
7 432 birds of their size (Alexander 1983a,b, Doube et al. 2012, Brassey et al. 2013). Hence, the  
8  
9 433 limb bones of moa are robust both inside and out. One hypothesis proposed to explain this is  
10  
11 434 that, since moa lacked any natural predators, they could afford to evolve more robust limb  
12  
13 435 bones that were more resistant to fracture, yet being heavier were more cumbersome to  
14  
15 436 move around (Alexander 1983b, 1985). This is incorrect, however, as abundant fossil  
16  
17 437 evidence indicates that moa were preyed upon by the extinct giant eagle *Harpagornis*  
18  
19 438 *moorei* Haast, 1872 (Worthy & Holdaway 1996, 2002). Increased bone robusticity could  
20  
21 439 alternatively be a mechanical adaptation to increased unpredictability of loads, providing a  
22  
23 440 higher factor of safety against accidental and extreme, but rare, loading regimes (Currey &  
24  
25 441 Alexander 1985, Blob et al. 2014). Yet, many of the more robust moa species lived in low-  
26  
27 442 relief, sparsely forested environments (Worthy & Holdaway 2002), where locomotor-  
28  
29 443 induced bone loading would be expected to be relatively predictable (Brassey et al. 2013).  
30  
31  
32  
33  
34  
35  
36  
37

38 445 Given that mechanical hypotheses have so far proven inadequate in explaining moa limb  
39  
40 446 bone robusticity, the possibility must be considered that one or more other, non-mechanical,  
41  
42 447 reasons exist. Moa had a unique suite of life history traits among birds, and it is possible that  
43  
44 448 this may have influenced limb bone robusticity. They had a strongly K-selected reproductive  
45  
46 449 strategy, with prolonged juvenile growth phases before reaching maturity (taking several  
47  
48 450 years, possibly even over a decade), and potentially living for a very long time thereafter  
49  
50 451 (Turvey & Holdaway 2005, Turvey et al. 2005). At least some species also exhibited  
51  
52 452 extreme reversed sexual size dimorphism, with females up to 280% larger than males  
53  
54 453 (Bunce et al. 2003, Huynen et al. 2003). Coupled with their large size, this raises the  
55  
56 454 possibility of heterochrony – in particular, hypermorphosis – playing an important role in  
57  
58  
59  
60

1  
2  
3 455 shaping the adult morphology of these birds (Churchill 1998, McNamara 2012). For a given  
4  
5 456 bone, the present study sampled two large individuals for each species, and for *D. robustus*  
6  
7  
8 457 and *P. elephantopus* at least it is known that only adult females were sampled here (Allentoft  
9  
10 458 et al. 2010). In addition to allometric effects and heterochrony, it may also be the case that  
11  
12 459 repeated deposition and resorption of medullary bone during each reproductive cycle over  
13  
14 460 many years may have had an effect on the morphologies observed here. Yet another  
15  
16 461 possibility is that strong seasonality in temperature, food availability or food quality in  
17  
18 462 Pleistocene–Holocene New Zealand (Anderson 1989, Worthy & Holdaway 2002) may have  
19  
20 463 resulted in moa undergoing marked annual fluctuations in body mass, with subsequent  
21  
22 464 effects on bone loading magnitudes and in turn bone adaptation. Currently these hypotheses  
23  
24 465 are purely speculative, yet by using a combination of CT and histological approaches, future  
25  
26 466 work should be able to investigate the above possibilities. This will require greatly expanded  
27  
28 467 sample sizes than that used here, incorporating material from both males and females, from a  
29  
30 468 wide range of ontogenetic stages and from a wide range of geographic localities.  
31  
32  
33  
34  
35  
36  
37

## 38 470 Conclusion

39  
40 471 The 3-D architecture of cancellous bone in the femur, tibiotarsus and fibula of three extinct  
41  
42 472 moa species is on the whole comparable to that of extant ground-dwelling birds, especially  
43  
44 473 larger species. Notwithstanding the small sample size of the present study, this would  
45  
46 474 suggest much similarity in posture and locomotor biomechanics between moa and extant  
47  
48 475 birds, which could be further clarified through computational modelling of whole-body  
49  
50 476 centre of mass location (e.g., Henderson 1999, Hutchinson et al. 2007, Bates et al. 2009) or  
51  
52 477 muscle moment arms (e.g., Hutchinson et al. 2005, Bates & Schachner 2012, Maidment et  
53  
54 478 al. 2014). By incorporating greater samples sizes and more species than that used in the  
55  
56 479 current study, future work may be able to refine the interpretations made here. Additionally,  
57  
58  
59  
60

1  
2  
3 480 such future studies could explicitly address the potential for phylogenetic influences on  
4  
5 481 cancellous bone architecture, which was not examined in the present study. Previously, it  
6  
7 482 was noted that comparably-sized small palaeognaths and neognaths showed similar  
8  
9 483 architectural patterns, suggesting minimal phylogenetic influence (Bishop et al. 2018b), but  
10  
11 484 whether this holds true at larger body size remains to be determined. One salient difference  
12  
13 485 between the cancellous bone architecture of moa and extant birds is the markedly greater  
14  
15 486 extent of cancellous bone in the diaphyses of the femur and tibiotarsus. The reason for the  
16  
17 487 great robusticity of moa limb bones, inside and out, may not be mechanical in nature, but  
18  
19 488 rather related to one or more aspects of their unique life history or environment.  
20  
21  
22  
23  
24  
25

## 26 490 Acknowledgements

27  
28 491 The staff of the Geosciences Program of the Queensland Museum are thanked for the  
29  
30 492 provision of workspace and access to literature. Access to the specimens studied was  
31  
32 493 provided by the Canterbury Museum, Christchurch. The invaluable assistance of M. Shaw,  
33  
34 494 C. Vink, D. Hely and the Christchurch Hospital Radiology Department with CT scanning is  
35  
36 495 gratefully acknowledged, as are the efforts of Ms M. Lloyd in obtaining literature. J.  
37  
38 496 Hutchinson, C. Clemente, D. Lloyd and R. Barrett provided helpful discussion of the topics  
39  
40 497 covered here. Special thanks are due to the volunteers who performed the categorical  
41  
42 498 scoring: R. Lawrence, J. Rasmussen, J. Macmillan, D. O'Boyle and N. Bishop. Likewise,  
43  
44 499 the constructive comments of two anonymous reviewers and the editor are much  
45  
46 500 appreciated, which helped to improve the clarity of the work presented here. This research  
47  
48 501 was supported in part by an Australian Government Research Training Program Scholarship  
49  
50 502 (to P.J.B., awarded by Griffith University), and the donation of CT scan time by the  
51  
52 503 Christchurch Hospital Radiology Department (to R.P.S.). Copies of the data used in this  
53  
54 504 study are held in the Geosciences Collection of the Queensland Museum and the Natural  
55  
56  
57  
58  
59  
60

1  
2  
3 505 History Collections of the Canterbury Museum. Additionally, 3-D models of each bone  
4  
5 506 studied can be viewed at [www.faanatoolkit.com](http://www.faanatoolkit.com). The authors declare no conflict of interest.  
6  
7

8 507

9  
10 508

11  
12 509 References

13  
14 510 ADACHI, T., TSUBOTA, K., TOMITA, Y. & HOLLISTER, S.J., 2001. Trabecular Surface  
15  
16 511 Remodeling Simulation for Cancellous Bone Using Microstructural Voxel Finite Element  
17  
18 512 Models. *Journal of Biomechanical Engineering* 123, 403–409.

19  
20 513 ALEXANDER, R.M., 1983a. Allometry of the leg bones of moas (*Dinornithes*) and other  
21  
22 514 birds. *Journal of Zoology* 200, 215–231.

23  
24 515 ALEXANDER, R.M., 1983b. On the massive legs of a Moa (*Pachyornis elephantopus*,  
25  
26 516 *Dinornithes*). *Journal of Zoology* 201, 363–376.

27  
28 517 ALEXANDER, R.M., 1985. The legs of ostriches (*Struthio*) and moas (*Pachyornis*). *Acta*  
29  
30 518 *Biotheoretica* 34, 165–174.

31  
32 519 ALLENTOFT, M.E., BUNCE, M., SCOFIELD, R.P., HALE, M.L. & HOLDAWAY, R.N., 2010.  
33  
34 520 Highly skewed sex ratios and biased fossil deposition of moa: ancient DNA provides new  
35  
36 521 insight on New Zealand's extinct megafauna. *Quaternary Science Reviews* 29, 753–762.

37  
38 522 ALLMENDINGER, R.W., CARDOZO, N.C. & FISHER, D., 2013. *Structural Geology Algorithms:*  
39  
40 523 *Vectors and Tensors*. Cambridge University Press, Cambridge, 289 pp.

41  
42 524 AMSON, E., ARNOLD, P., VAN HETEREN, A.H., CANOVILLE, A. & NYAKATURA, J.A., 2017.  
43  
44 525 Trabecular architecture in the forelimb epiphyses of extant xenarthrans (Mammalia).  
45  
46 526 *Frontiers in Zoology* 14, 52.

47  
48 527 ANDERSON, A.J., 1989. *Prodigious Birds: Moas and Moa-Hunting in Prehistoric New*  
49  
50 528 *Zealand*. Cambridge University Press, Cambridge, 238 pp.

- 1  
2  
3 529 BARAK, M.M., LIEBERMAN, D.E. & HUBLIN, J.-J., 2011. A Wolff in sheep's clothing:  
4  
5 530 Trabecular bone adaptation in response to changes in joint loading orientation. *Bone* 49,  
6  
7 531 1141–1151.  
8  
9  
10 532 BARAK, M.M., LIEBERMAN, D.E., RAICHLIN, D.A., PONTZER, H., WARRENER, A.G. &  
11  
12 533 HUBLIN, J.-J., 2013. Trabecular Evidence for a Human-Like Gait in *Australopithecus*  
13  
14 534 *africanus*. *PLOS ONE* 8, e77687.  
15  
16  
17 535 BATES, K.T. & SCHACHNER, E.R., 2012. Disparity and convergence in bipedal archosaur  
18  
19 536 locomotion. *Journal of the Royal Society Interface* 9, 1339–1353.  
20  
21 537 BATES, K.T., MANNING, P.L., HODGETTS, D. & SELLERS, W.I., 2009. Estimating Mass  
22  
23 538 Properties of Dinosaurs Using Laser Imaging and 3D Computer Modelling. *PLOS ONE*  
24  
25 539 4, e4532.  
26  
27  
28 540 BIEWENER, A.A., 1989. Scaling Body Support in Mammals: Limb Posture and Muscle  
29  
30 541 Mechanics. *Science* 245, 45–48.  
31  
32  
33 542 BIEWENER, A.A., FAZZALARI, N.L., KONIECZYNSKI, D.D. & BAUDINETTE, R.V., 1996.  
34  
35 543 Adaptive Changes in Trabecular Architecture in Relation to Functional Strain Patterns  
36  
37 544 and Disuse. *Bone* 19, 1–8.  
38  
39  
40 545 BISHOP, P.J., 2015. A critical re-evaluation of the hindlimb myology of moa (Aves:  
41  
42 546 *Dinornithiformes*). *Memoirs of the Queensland Museum* 59, 187–246.  
43  
44  
45 547 BISHOP, P.J., GRAHAM, D.F., LAMAS, L.P., HUTCHINSON, J.R., RUBENSON, J., HANCOCK, J.A.,  
46  
47 548 WILSON, R.S., HOCKNULL, S.A., BARRETT, R.S., LLOYD, D.G. & CLEMENTE, C.J., 2018a.  
48  
49 549 The Influence of Speed and Size on Avian Terrestrial Locomotor Biomechanics:  
50  
51 550 Predicting Locomotion in Extinct Theropod Dinosaurs. *PLOS ONE* 13, e0192172.  
52  
53  
54 551 BISHOP, P.J., HOCKNULL, S.A., CLEMENTE, C.J., HUTCHINSON, J.R., FARKE, A.A., BECK,  
55  
56 552 B.R., BARRETT, R.S. & LLOYD, D.G., 2018b. Cancellous bone architecture and theropod  
57  
58  
59  
60

1  
2  
3 553 dinosaur locomotion. Part I – An examination of cancellous bone architecture in the  
4  
5 554 hindlimb bones of theropods. PeerJ 6, e5778.  
6  
7  
8 555 BLOB R. W., ESPINOZA, N.R., BUTCHER, M. T., LEE, A.H., D’AMICO, A.R., BAIG, F. &  
9  
10 556 SHEFFIELD, K.M., 2014. Diversity of Limb-Bone Safety Factors for Locomotion in  
11  
12 557 Terrestrial Vertebrates: Evolution and Mixed Chains. Integrative and Comparative  
13  
14 558 Biology 54, 1058–1071.  
15  
16  
17 559 BOYLE, C. & KIM, I.Y., 2011. Three-dimensional micro-level computational study of  
18  
19 560 Wolff’s law via trabecular bone remodeling in the human proximal femur using design  
20  
21 561 space topology optimization. Journal of Biomechanics 44, 935–942.  
22  
23  
24 562 BRASSEY, C.A., HOLDAWAY, R.N., PACKHAM, A.G., ANNÉ, J., MANNING, P.L. & SELLERS,  
25  
26 563 W.I., 2013. More than one way of being a moa: Differences in leg bone robustness map  
27  
28 564 divergent evolutionary trajectories in Dinornithidae and Emeidae (Dinornithiformes).  
29  
30 565 PLOS ONE 8, e82668.  
31  
32  
33 566 BUNCE, M., WORTHY, T.H., FORD, T., HOPPITT, W., WILLERSLEV, E., DRUMMOND, A. &  
34  
35 567 COOPER, A., 2003. Extreme reversed sexual size dimorphism in the extinct New Zealand  
36  
37 568 moa *Dinornis*. Nature 425, 172–175.  
38  
39  
40 569 BUTLER, R.F., 1992. Paleomagnetism: Magnetic Domains to Geological Terranes.  
41  
42 570 Blackwell Scientific, Oxford, 238 pp.  
43  
44  
45 571 CARDOZO, N.C. & ALLMENDINGER, R.W., 2013. Spherical projections with OSXStereonet.  
46  
47 572 Computers & Geosciences 51, 193–205.  
48  
49 573 CHRISTEN, P., ITO, K., DOS SANTOS, A.A., MÜLLER, R. & VAN RIETBERGEN, B., 2013.  
50  
51 574 Validation of a bone loading estimation algorithm for patient-specific bone remodelling  
52  
53 575 simulations. Journal of Biomechanics 46, 941–948.  
54  
55  
56 576 CHURCHILL, S.E., 1998. Cold Adaptation, Heterochrony, and Neandertals. Evolutionary  
57  
58 577 Anthropology 7, 46–61.  
59  
60

- 1  
2  
3 578 CLEMENTE, C.J., THOMPSON, G.G. & WITHERS, P.C., 2009. Evolutionary relationships of  
4  
5 579 sprint speed in Australian varanid lizards. *Journal of Zoology* 278, 270–280.  
6  
7  
8 580 COWIN, S.C., 1986. Wolff's Law of Trabecular Architecture at Remodelling Equilibrium.  
9  
10 581 *Journal of Biomechanical Engineering* 108, 83–88.  
11  
12 582 CRUZ-ORIVE, L.M., KARLSSON, L.M., LARSEN, S.E. & WAINSCHEIN, F., 1992.  
13  
14 583 Characterizing anisotropy: a new concept. *Micron and Microscopica Acta* 23, 75–76.  
15  
16  
17 584 CURREY, J.D. & ALEXANDER, R.M., 1985. The thickness of the walls of tubular bones.  
18  
19 585 *Journal of Zoology* 206, 453–468.  
20  
21 586 DEMES, B., 2007. In vivo bone strain and bone functional adaptation. *American Journal of*  
22  
23 587 *Physical Anthropology* 133, 717–722.  
24  
25  
26 588 DEMES, B., QIN, Y.-X., STERN, J.T., JR, LARSON, S.G. & RUBIN, C.T., 2001. Patterns of strain  
27  
28 589 in the macaque tibia during functional activity. *American Journal of Physical*  
29  
30 590 *Anthropology* 116, 257–265.  
31  
32  
33 591 DEMES, B., STERN, J.T., JR, HAUSMAN, M.R., LARSON, S.G., MCLEOD, K.J. & RUBIN, C.T.,  
34  
35 592 1998. Patterns of strain in the macaque ulna during functional activity. *American Journal*  
36  
37 593 *of Physical Anthropology* 106, 87–100.  
38  
39  
40 594 DICK, T.J.M. & CLEMENTE, C.J., 2017. Where have All the Giants Gone? How Animals Deal  
41  
42 595 with the Problem of Size. *PLOS Biology* 15, e2000473.  
43  
44  
45 596 DOUBE, M., YEN, S.C.W., KŁOSOWSKI, M.M., FARKE, A.A., HUTCHINSON, J.R. &  
46  
47 597 SHEFELBINE, S.J., 2012. Whole-bone scaling of the avian pelvic limb. *Journal of Anatomy*  
48  
49 598 221, 21–29.  
50  
51 599 FAJARDO, R.J. & MÜLLER, R., 2001. Three-Dimensional Analysis of Nonhuman Primate  
52  
53 600 Trabecular Architecture Using Micro-Computed Tomography. *American Journal of*  
54  
55 601 *Physical Anthropology* 115, 327–336.  
56  
57  
58  
59  
60

- 1  
2  
3 602 FYHRIE, D.P. & CARTER, D.R., 1986. A Unifying Principle Relating Stress to Trabecular  
4  
5 603 Bone Morphology. *Journal of Orthopaedic Research* 4, 304–317.  
6  
7  
8 604 GARLAND, T., JR, 1983. The relation between maximal running speed and body mass in  
9  
10 605 terrestrial mammals. *Journal of Zoology* 199, 157–170.  
11  
12 606 GATESY, S.M. & BIEWENER, A.A., 1991. Bipedal locomotion: effects of speed, size and limb  
13  
14 607 posture in birds and humans. *Journal of Zoology* 224, 127–147.  
15  
16  
17 608 GATESY, S.M. & MIDDLETON, K.M., 1997. Bipedalism, flight, and the evolution of theropod  
18  
19 609 locomotor diversity. *Journal of Vertebrate Paleontology* 17, 308–329.  
20  
21  
22 610 GEORGIU, L., KIVELL, T.L., PAHR, D.H. & SKINNER, M.M., 2018. Trabecular bone  
23  
24 611 patterning in the hominoid distal femur. *PeerJ* 6, e5156.  
25  
26  
27 612 GOLDSTEIN, S.A., MATTHEWS, L.S., KUHN, J.L. & HOLLISTER, S.J., 1991. Trabecular bone  
28  
29 613 remodelling: an experimental model. *Journal of Biomechanics* 24 (suppl. 1), 135–150.  
30  
31  
32 614 HAAST, J., 1872. Notes on *Harpagornis moorei*, an Extinct Gigantic Bird of Prey, containing  
33  
34 615 Description of Femur, Ungual Phalanges, and Rib. *Transactions and Proceedings of the*  
35  
36 616 *New Zealand Institute* 4, 192–196.  
37  
38  
39 617 HAMMER, Ø., HARPER, D.A.T. & RYAN, P.D., 2001. PAST: Paleontological Statistics  
40  
41 618 Software Package for Education and Data Analysis. *Palaeontologia Electronica* 4, 4.  
42  
43  
44 619 HÉBERT, D., LEBRUN, R. & MARIVAUX, L., 2012. Comparative Three-Dimensional Structure  
45  
46 620 of the Trabecular Bone in the Talus of Primates and Its Relationship to Ankle Joint Loads  
47  
48 621 Generated During Locomotion. *The Anatomical Record* 295, 2069–2088.  
49  
50  
51 622 HENDERSON, D.M., 1999. Estimating the masses and centers of mass of extinct animals by  
52  
53 623 3-D mathematical slicing. *Paleobiology* 25, 88–106.  
54  
55  
56 624 HUISKES, R., RUIJERMAN, R., VAN LENTHE, G.H. & JANSSEN, J.D., 2000. Effects of  
57  
58 625 mechanical forces on maintenance and adaptation of form in trabecular bone. *Nature* 405,  
59  
60 626 704–706.

- 1  
2  
3 627 HUTCHINSON, J.R., 2004. Biomechanical Modeling and Sensitivity Analysis of Bipedal  
4  
5 628 Running Ability. II. Extinct Taxa. *Journal of Morphology* 262, 441–461.  
6  
7  
8 629 HUTCHINSON, J.R., ANDERSON, F.C., BLEMKER, S.S. & DELP, S.L., 2005. Analysis of  
9  
10 630 hindlimb muscle moment arms in *Tyrannosaurus rex* using a three-dimensional  
11  
12 631 musculoskeletal computer model: implications for stance, gait, and speed. *Paleobiology*  
13  
14 632 31, 676–701.  
15  
16  
17 633 HUTCHINSON, J.R., FAMINI, D., LAIR, R. & KRAM, R., 2003. Are fast-moving elephants really  
18  
19 634 running? *Nature* 422, 493–494.  
20  
21  
22 635 HUTCHINSON, J.R. & GATESY, S.M., 2006. Dinosaur locomotion: Beyond the bones. *Nature*  
23  
24 636 440, 292–294.  
25  
26  
27 637 HUTCHINSON, J.R., NG-THOW-HING, V. & ANDERSON, F.C., 2007. A 3D interactive method  
28  
29 638 for estimating body segmental parameters in animals: Application to the turning and  
30  
31 639 running performance of *Tyrannosaurus rex*. *Journal of Theoretical Biology* 246, 660–  
32  
33 640 6800.  
34  
35  
36 641 HUYNEN, L., MILLAR, C.D., SCOFIELD, R.P. & LAMBERT, D.M., 2003. Nuclear DNA  
37  
38 642 sequences detect species limits in ancient moa. *Nature* 425, 175–178.  
39  
40  
41 643 KETCHAM, R.A. & RYAN, T.M., 2004. Quantification and visualization of anisotropy in  
42  
43 644 trabecular bone. *Journal of Microscopy* 213, 158–171.  
44  
45  
46 645 KIVELL, T.L., 2016. A review of trabecular bone functional adaptation: what have we  
47  
48 646 learned from trabecular analyses in extant hominoids and what can we apply to fossils?  
49  
50 647 *Journal of Anatomy* 228, 569–594.  
51  
52  
53 648 LEGENDRE, P. & LEGENDRE, L., 2012. *Numerical Ecology*, Third English Edition. Elsevier,  
54  
55 649 Amsterdam, 1006 pp.  
56  
57  
58 650 LIEBERMAN, D.E., POLK, J.D. & DEMES, B., 2004. Predicting Long Bone Loading From  
59  
60 651 Cross-Sectional Geometry. *American Journal of Physical Anthropology* 123, 156–171.

- 1  
2  
3 652 MAGA, M., KAPPELMAN, J., RYAN, T.M. & KETCHAM, R.A., 2006. Preliminary Observations  
4  
5 653 on the Calcaneal Trabecular Microarchitecture of Extant Large-Bodied Hominoids.  
6  
7 654 American Journal of Physical Anthropology 129, 410–417.  
8  
9  
10 655 MAIDMENT, S.C.R., BATES, K.T., FALKINGHAM, P.L., VANBUREN, C., ARBOUR, V. &  
11  
12 656 BARRETT, P.M., 2014. Locomotion in ornithischian dinosaurs: an assessment using three-  
13  
14 657 dimensional computational modelling. Biological Review, 89, 588–617.  
15  
16  
17 658 MAIN, R.P. & BIEWENER, A.A., 2004. Ontogenetic patterns of limb loading, in vivo bone  
18  
19 659 strains and growth in the goat radius. Journal of Experimental Biology, 207, 2577–2588.  
20  
21 660 MATARAZZO, S.A., 2015. Trabecular Architecture of the Manual Elements Reflects  
22  
23 661 Locomotor Patterns in Primates. PLOS ONE 10, e0120436.  
24  
25  
26 662 MCNAMARA, K.J., 2012. Heterochrony: the Evolution of Development. Evolution:  
27  
28 663 Education and Outreach 5, 203–218.  
29  
30  
31 664 MULLENDER, M.G. & HUISKES, R., 1995. Proposal for the Regulatory Mechanism of Wolff's  
32  
33 665 Law. Journal of Orthopaedic Research 13, 503–512.  
34  
35  
36 666 MURRAY, P.F. & VICKERS-RICH, P., 2004. Magnificent Mihirungs: The Colossal Flightless  
37  
38 667 Birds of the Australian Dreamtime, Indiana University Press, Bloomington.  
39  
40 668 ODGAARD, A., 1997. Three-Dimensional Methods for Quantification of Cancellous Bone  
41  
42 669 Architecture. Bone 20, 315–328.  
43  
44  
45 670 ODGAARD, A., 2001. Quantification of Cancellous Bone Architecture. In Bone Biomechanics  
46  
47 671 Handbook. COWIN, S.C., ed., CRC Press, Boca Raton, pp. 14-1–14-19.  
48  
49 672 OWEN, R., 1844. On Dinornis, an extinct genus of tridactyle struthious birds, with  
50  
51 673 descriptions of portions of the skeleton of five species which formerly existed in  
52  
53 674 NewZealand (Part I). Transactions of the Zoological Society of London 3, 235–275.  
54  
55  
56 675 OWEN, R., 1846. On Dinornis (Part II), containing descriptions of portions of the skull, the  
57  
58 676 sternum and other parts of the skeleton of the species previously determined, with  
59  
60

- 1  
2  
3 677 osteological evidences of three additional species, and a new genus, *Palapteryx*.  
4  
5 678 Transactions of the Zoological Society of London 3, 307–329.  
6  
7  
8 679 OWEN, R., 1858. On *Dinornis* (Part VII): containing a description of the bones of the leg and  
9  
10 680 foot of *Dinornis elephantopus*, Owen. Transactions of the Zoological Society of London  
11  
12 681 5, 149–158.  
13  
14 682 OWEN, R., 1883. On *Dinornis* (Part XXIII): containing a description of the head and feet with  
15  
16 683 their dried integuments, of an individual of the species *Dinornis didinus* Owen.  
17  
18 684 Transactions of the Zoological Society of London 11, 257–261.  
19  
20 685 PEARSON, O.M. & LIEBERMAN, D.E., 2004. The Aging of Wolff's "Law": Ontogeny and  
21  
22 686 Responses to Mechanical Loading in Cortical Bone. *Yearbook of Physical Anthropology*,  
23  
24 687 47, 63–99.  
25  
26 688 POLK, J.D., BLUMENFELD, J. & AHLUWALIA, D., 2008. Knee Posture Predicted From  
27  
28 689 Subchondral Apparent Density in the Distal Femur: An Experimental Validation. *The*  
29  
30 690 *Anatomical Record* 16, 323–329.  
31  
32 691 PONTZER, H., LIEBERMAN, D.E., MOMIN, E., DEVLIN, M.J., POLK, J.D., HALLGRÍMSSON, B. &  
33  
34 692 COOPER, D.M.L., 2006. Trabecular bone in the bird knee responds with high sensitivity to  
35  
36 693 changes in load orientation. *Journal of Experimental Biology* 209, 57–65.  
37  
38 694 RADIN, E.L., ORR, R.B., KELMAN, J.L., PAUL, I.L. & ROSE, R.M., 1982. Effect of prolonged  
39  
40 695 walking on concrete on the knees of sheep. *Journal of Biomechanics* 15, 487–492.  
41  
42 696 RUIJTERMAN, R., HILBERS, P., VAN RIETBERGEN, B. & HUISKES, R., 2005. A theoretical  
43  
44 697 framework for strain-related trabecular bone maintenance and adaptation. *Journal of*  
45  
46 698 *Biomechanics* 38, 931–941.  
47  
48 699 RYAN, T.M. & KETCHAM, R.A., 2002a. Femoral head trabecular bone structure in two  
49  
50 700 omomyid primates. *Journal of Human Evolution* 43, 241–263.  
51  
52  
53  
54  
55  
56  
57  
58  
59  
60

- 1  
2  
3 701 RYAN, T.M. & KETCHAM, R.A., 2002b. The three-dimensional structure of trabecular bone  
4  
5 702 in the femoral head of strepsirrhine primates. *Journal of Human Evolution* 43, 1–26.  
6  
7  
8 703 RYAN, T.M. & KETCHAM, R.A., 2005. Angular Orientation of Trabecular Bone in the  
9  
10 704 Femoral Head and Its Relationship to Hip Joint Loads in Leaping Primates. *Journal of*  
11  
12 705 *Morphology* 265, 249–263.  
13  
14  
15 706 RYAN, T.M. & SHAW, C.N., 2012. Unique Suites of Trabecular Bone Features Characterize  
16  
17 707 Locomotor Behavior in Human and Non-Human Anthropoid Primates. *PLOS ONE* 7,  
18  
19 708 e41037.  
20  
21  
22 709 SELLERS, W.I. & MANNING, P.L., 2007. Estimating dinosaur maximum running speeds using  
23  
24 710 evolutionary robotics. *Proceedings of the Royal Society of London, Series B* 274, 2711–  
25  
26 711 2716.  
27  
28  
29 712 SU, A., WALLACE, I.J. & NAKATSUKASA, M., 2013. Trabecular bone anisotropy and  
30  
31 713 orientation in an Early Pleistocene hominin talus from East Turkana, Kenya. *Journal of*  
32  
33 714 *Human Evolution* 64, 667–677.  
34  
35  
36 715 THOMASON, J.J., 1995. To what extent can the mechanical environment of a bone be inferred  
37  
38 716 from its internal architecture? In *Functional Morphology in Vertebrate Paleontology* (ed  
39  
40 717 Thomason JJ), pp. 249–263. New York: Cambridge University Press.  
41  
42  
43 718 THULBORN, T., 1990. *Dinosaur Tracks*. Chapman and Hall, London, 410 pp.  
44  
45  
46 719 TSEGAI, Z.J., KIVELL, T.L., GROSS, T., NGUYEN, N.H., PAHR, D.H., SMAERS, J.B. & SKINNER,  
47  
48 720 M.M., 2013. Trabecular Bone Structure Correlates with Hand Posture and Use in  
49  
50 721 Hominoids. *PLOS ONE* 8, e78781.  
51  
52  
53 722 TURVEY, S.T., GREEN, O.R. & HOLDAWAY, R.N., 2005. Cortical growth marks reveal  
54  
55 723 extended juvenile development in New Zealand moa. *Nature* 435, 940–943.  
56  
57  
58 724 TURVEY, S.T. & HOLDAWAY, R.N., 2005. Postnatal ontogeny, population structure, and  
59  
60 725 extinction of the giant moa *Dinornis*. *Journal of Morphology* 265, 70–86.

- 1  
2  
3 726 VAN DER MEULEN, M.C.H., MORGAN, T.G., YANG, X., BALDINI, T.H., MYERS, E.R., WRIGHT,  
4  
5 727 T.M. & BOSTROM, M.P.G., 2006. Cancellous bone adaptation to in vivo loading in a  
6  
7 728 rabbit model. *Bone* 38, 871–877.
- 9  
10 729 VOLPATO, V., VIOLA, T.B., NAKATSUSAKA, M., BONDIOLI, L. & MACCHIARELLI, R., 2008.  
11  
12 730 Textural characteristics of the iliac-femoral trabecular pattern in a bipedally trained  
13  
14 731 Japanese macaque. *Primates* 49, 16–25.
- 16  
17 732 WALLACE, I.J., DEMES, B., MONGLE, C., PEARSON, O.M., POLK, J.D. & LIEBERMAN, D.E.,  
18  
19 733 2014. Exercise-Induced Bone Formation is Poorly Linked to Local Strain Magnitude in  
20  
21 734 the Sheep Tibia. *PLOS ONE* 9, e99108.
- 23  
24 735 WANG, H., JI, B., LIU, X.S., GUO, X.E., HUANG, Y. & HWANG, K.-C., 2012. Analysis of  
25  
26 736 microstructural and mechanical alterations of trabecular bone in a simulated three-  
27  
28 737 dimensional remodelling process. *Journal of Biomechanics* 45, 2417–2425.
- 30  
31 738 WORTHY, T.H., 1989. Aspects of the biology of two moa species (Aves: Dinornithiformes).  
32  
33 739 *New Zealand Journal of Archaeology* 11, 77–86.
- 35  
36 740 WORTHY, T.H. & HOLDAWAY, R.N., 1996. Quaternary fossil faunas, overlapping  
37  
38 741 taphonomies, and palaeofaunal reconstruction in North Canterbury, South Island, New  
39  
40 742 Zealand. *Journal of the Royal Society of New Zealand* 26, 275–361.
- 42  
43 743 WORTHY, T.H. & HOLDAWAY, R.N., 2002. *The Lost World of the Moa*. Indiana University  
44  
45 744 Press, Bloomington, 718 pp.
- 47  
48 745 WORTHY, T.H. & SCOFIELD, R.P., 2012. Twenty-first century advances in knowledge of the  
49  
50 746 biology of moa (Aves: Dinornithiformes): a new morphological analysis and moa  
51  
52 747 diagnoses revised. *New Zealand Journal of Zoology* 39, 87–153.
- 53  
54 748 ZINOVIEV, A.V., 2013. Notes on the pelvic and hindlimb myology and syndesmology of  
55  
56 749 *Emeus crassus* and *Dinornis robustus* (Aves: Dinornithiformes). In *Eighth International*

1  
2  
3 750 Meeting of the Society of Avian Paleontology and Evolution, Vienna, 11–16 June, 2012.

4  
5 751 GÖHLICH, U.B. & KROH, A., eds, Naturhistorisches Museum Wien, Vienna, 253–278.

6  
7  
8 752

9  
10 753

11  
12 754 Figure captions

13  
14  
15 755

16  
17 756 Fig. 1. The main architectural features of cancellous bone in the proximal femur of moa. A,

18  
19 757 B, vector field of  $u_1$  in the femoral head and inferior neck of *D. robustus* (CM Av8488)

20  
21 758 plotted on a translucent rendering of the external bony geometry, in anterior (A) and medial

22  
23 759 (B) views. C, D, vector field of  $u_1$  under the facies antitrochanterica of *P. elephantopus* (CM

24  
25 760 Av 8716), in posterior (C) and lateral (D) views. E, F, vector field of  $u_1$  in the trochanteric

26  
27 761 crest of *M. didinus* (CM Av8507J), in anterior (E) and lateral (F) views. G, H, vector field

28  
29 762 of  $u_1$  in the trochanteric crest of *D. robustus* (CM Av 8488), in anterior (G) and lateral (H)

30  
31 763 views. In this and all subsequent illustrations of fabric vector fields, all images are of bones

32  
33 764 from the right side of the body.

34  
35  
36  
37 765

38  
39 766 Fig. 2. The main architectural features of cancellous bone in the distal femur of moa. A,

40  
41 767 vector field of  $u_1$  in the central metaphysis of *D. robustus* (CM Av 8422), in a 3-D slice,

42  
43 768 parallel to the sagittal plane and between the condyles, shown in lateral view. Schematic

44  
45 769 inset illustrates the modestly developed double-arcuate pattern. B, vector field of  $u_1$  in the

46  
47 770 central metaphysis of *P. elephantopus* (CM Av15029), in a 3-D slice, parallel to the coronal

48  
49 771 plane, shown in anterior view. Schematic inset illustrates the ‘radiating’ pattern. C, D, vector

50  
51 772 field of  $u_1$  in the medial condyle of *P. elephantopus* (CM Av8716), shown in anterior (C)

52  
53 773 and medial (D) views. E, F, vector field of  $u_1$  in the lateral condyle of *D. robustus* (CM

54  
55 774 Av8422), shown in anterior (E) and lateral (F) views. G, vector field of  $u_2$  in a 3-D slice

1  
2  
3 775 through the middle of the condyles in *M. didinus* (CM Av8507O), shown in distal view.

4  
5 776 Schematic inset illustrates the ‘butterfly’ pattern.

6  
7  
8 777

9  
10 778 Fig. 3. Examples of increased disorganization or obliquity in the vector field of  $u_1$  in the

11  
12 779 femoral metaphyses. A, proximal femoral metaphysis of *D. robustus* (CM Av8422). B,

13  
14 780 distal femoral metaphysis of *M. didinus* (CM Av8507J). Regions of increased

15  
16  
17 781 disorganization are indicated by the braces.

18  
19 782

20  
21 783 Fig. 4. The mean orientation of  $u_1$  in the femoral head and medial femoral condyle of moa

22  
23 784 and extant birds, referenced in an explicit anatomical coordinate system. A, the mean

24  
25 785 directions as plotted on an equal-angle stereoplot (using StereoNet 9.5; Allmendinger et al.

26  
27 786 2013, Cardozo and Allmendinger, 2013). The data for the femoral head are plotted with a

28  
29 787 northern hemisphere projection, and are shown as filled symbols; the data for the medial

30  
31 788 femoral condyle are plotted with a southern hemisphere projection, and are shown as hollow

32  
33 789 symbols. Grey symbols are extant birds as reported previously (Bishop et al. 2018b), black

34  
35 790 symbols are moa; for moa, squares represent *D. robustus*, triangles represent *P.*

36  
37 791 elephantopus and diamonds represent *M. didinus*. For each dataset, the large circle symbol

38  
39 792 indicates the mean direction across the group, and the surrounding dotted line indicates the

40  
41 793 95% confidence cone about the mean. B, comparison of the anterior inclination of  $u_1$  in the

42  
43 794 sagittal plane of the femoral head versus femur length in moa and extant birds. C,

44  
45 795 comparison of the posterior inclination of  $u_1$  in the sagittal plane of the medial femoral

46  
47 796 condyle versus femur length in moa and extant birds. In both B and C, the data for extant

48  
49 797 birds are as reported previously (Bishop et al. 2018b) and are shown in grey, whereas the

50  
51 798 data for moa are shown in black, with the same symbols as for A. Major axis regressions are

52  
53 799 plotted and associated statistics are shown.

800

801 Fig. 5. The main architectural features of cancellous bone in the proximal tibiotarsus of moa.

802 A, B, vector field of  $u_1$  in the cranial and lateral cnemial crests of *D. robustus* (CM Av8488)

803 shown in anterior (A) and medial (B) views. C, D, vector field of  $u_1$  under the medial

804 condyle of *M. didinus* (CM Av8513T) shown in posterior (C) and medial (D) views. E, F,

805 vector field of  $u_1$  under the lateral condyle of *P. elephantopus* (CM Av8383) shown in

806 posterior (E) and lateral (F) views. G, vector field of  $u_1$  in a 3-D slice through the middle of

807 the proximal metaphysis, cnemial crests and condyles of *D. robustus* (CM Av8422), parallel

808 to the sagittal plane and shown in medial view. Schematic inset illustrates the well-

809 developed double-arcuate pattern present. H, vector field of  $u_1$  throughout the entire

810 proximal tibia of *P. elephantopus* (CM Av8716), shown in medial view, illustrating

811 increased obliquity and disorganization of vectors in the distal metaphysis and transition to

812 the diaphysis (region with braces).

813

814 Fig. 6. The main architectural features of cancellous bone in the distal tibiotarsus of moa. A–

815 D, vector field of  $u_1$  (A, C) and  $u_2$  (B, D) in the distal tibiotarsus of *P. elephantopus* (CM

816 Av8383) in oblique anterolateral (A, B) and oblique anteromedial (C, D) views. E, vector

817 field of  $u_1$  (black) and  $u_2$  (white) in the condyles of *P. elephantopus* (CM Av8383) in

818 proximal view. Note how both  $u_1$  and  $u_2$  are aligned approximately parallel to the sagittal

819 plane. F, isosurface rendering of cancellous bone in the distal tibiotarsus of *D. robustus* (CM

820 Av8488), shown in oblique anterolateral view, with multiple cuts through the bone to

821 illustrate the 3-D architecture. Cut surfaces are coloured black to better illustrate the nature

822 of the cancellous bone architecture, in particular the plate-like nature of many trabeculae,

823 largely aligned parallel to the sagittal plane.

824

1  
2  
3 825 Fig. 7. The main architectural features of cancellous bone in the proximal fibula of moa, as  
4  
5 826 exemplified here by *D. robustus* (CM Av8490), which shows the vector field of  $u_1$  in lateral  
6  
7 827 view.  
8  
9

10 828

11  
12 829 Fig. 8. Size-dependent variation in the nature of diaphyseal cancellous bone architecture in  
13  
14 830 the femora and tibiae of moa compared to extant birds. A, B, the extent of cancellous bone  
15  
16 831 in the femur (A) and tibia (B); a higher score indicates greater extent. C, D, the degree of  
17  
18 832 association of trabeculae with one another in the femur (C) and tibia (D); a higher score  
19  
20 833 indicates that trabeculae tend to be more closely associated with other trabeculae of similar  
21  
22 834 character. E, F, the average orientation of trabeculae in the femur (E) and tibia (F); a higher  
23  
24 835 score indicates that trabeculae are at a higher angle to the bone's long axis. The data for  
25  
26 836 extant birds are as reported previously (Bishop et al. 2018b) and are shown in grey; data for  
27  
28 837 moa are shown in black, with the same symbols as for Fig. 4. The major axis regression  
29  
30 838 lines derived for the whole data set are also plotted as solid lines; regression statistics are  
31  
32 839 reported in Table 2. Additionally plotted in A and B are the major axis regressions derived  
33  
34 840 previously for just the extant bird sample (dashed lines); these demonstrate that moa  
35  
36 841 diaphyses almost ubiquitously have a greater quantity of cancellous bone than would be  
37  
38 842 predicted for their size based on extant birds.  
39  
40  
41  
42  
43  
44  
45  
46

47 843

48 844 Fig. 9. Cancellous bone in the diaphyses of moa, illustrated here with several examples  
49  
50 845 illustrating the variety of manifestations it can assume. A, femur of *D. robustus* (CM  
51  
52 846 Av8488); see also Supplementary Movie S1. B, proximal tibiotarsus of *D. robustus* (CM  
53  
54 847 Av8488). C, femur of *P. elephantopus* (CM Av8716). D, proximal tibiotarsus of *P.*  
55  
56 848 *elephantopus* (CM Av8716). Note especially the abundant, oblique trabeculae throughout  
57  
58 849 the diaphysis of the femur. In all figures, proximal is towards the top of the page. In C, the  
59  
60

1  
2  
3 850 asterisk denotes a core produced during the extraction of cortical bone for genetic sampling  
4  
5 851 (Allentoft et al. 2010).  
6  
7

8 852  
9

10 853 Supplementary material  
11

12 854  
13

14 855 Movie S1. Animated isosurface rendering of the femur of *Dinornis robustus* (CM Av8488),  
15  
16

17 856 to illustrate the architecture and extent of cancellous bone in the diaphysis. For scale, the  
18

19 857 total length of the bone (vertical axis in the video) is 339 mm.  
20  
21  
22  
23  
24  
25  
26  
27  
28  
29  
30  
31  
32  
33  
34  
35  
36  
37  
38  
39  
40  
41  
42  
43  
44  
45  
46  
47  
48  
49  
50  
51  
52  
53  
54  
55  
56  
57  
58  
59  
60

1  
2  
3  
4  
5  
6  
7  
8  
9  
10  
11  
12  
13  
14  
15  
16  
17  
18  
19  
20  
21  
22  
23  
24  
25  
26  
27  
28  
29  
30  
31  
32  
33  
34  
35  
36  
37  
38  
39  
40  
41

Tables

Table 1. The specimens investigated in this study, as well the settings used in acquiring the CT scan data for each specimen. All specimens are curated in the Natural History Collections of the Canterbury Museum.

Species	Specimen number	Element	CT scan settings				
			Peak tube voltage (kV)	Tube current (mA)	Exposure time (ms)	In-plane pixel resolution (mm)*	Slice thickness (mm)*
Dinornis robustus	CM Av8422	femur	80, 140	189	1,000	0.498	0.4
Dinornis robustus	CM Av8422	tibiotarsus	80, 140	199	1,000	0.551	0.4
Dinornis robustus	CM Av8488	femur	80, 140	221	1,000	0.553	0.6
Dinornis robustus	CM Av8488	tibiotarsus	80, 140	221	1,000	0.816	0.6
Dinornis robustus	CM Av8488	fibula	80, 140	199	1,000	0.551	0.4
Dinornis robustus	CM Av8490	fibula	80, 140	199	1,000	0.551	0.4
Pachyornis elephantopus	CM Av8383	tibiotarsus	80, 140	200	1,000	0.551	0.4
Pachyornis elephantopus	CM Av8383	fibula	80, 140	200	1,000	0.551	0.4
Pachyornis elephantopus	CM Av8716	femur	80, 140	180	1,000	0.498	0.4
Pachyornis elephantopus	CM Av8716	tibiotarsus	80, 140	201	1,000	0.551	0.4
Pachyornis elephantopus	CM Av8716	fibula	80, 140	200	1,000	0.551	0.4
Pachyornis elephantopus	CM Av15029	femur	80, 140	159	1,000	0.498	0.4
Megalapteryx didinus	CM Av8507J	femur	80, 140	201	1,000	0.551	0.4
Megalapteryx didinus	CM Av8507O	femur	80, 140	201	1,000	0.551	0.4
Megalapteryx didinus	CM Av8513P	tibiotarsus	80, 140	200	1,000	0.551	0.4
Megalapteryx didinus	CM Av8513T	tibiotarsus	80, 140	201	1,000	0.551	0.4
Megalapteryx didinus	CM Av8506E	fibula	80, 140	201	1,000	0.551	0.4
Megalapteryx didinus	CM Av8506N	fibula	80, 140	201	1,000	0.551	0.4

\*The scans were processed according to protocol 2 of Bishop et al. (2018b), whereby the resulting images were of an isotropic voxel resolution equal to one third of the original in-plane pixel resolution.

44  
45  
46



Table 2. Statistical results of categorical scoring analyses of cancellous bone architecture in moa and extant bird femora and tibiotarsi versus bone length (in mm).

Element	Feature	Slope	Intercept	r <sup>2</sup>	p
Femur	extent	0.005733	0.2395	0.5624	< 0.0001
	association	0.002625	0.8782	0.3176	<0.0001
	orientation	-0.005919	6.4007	0.2680	0.0002
Tibiotarsus	extent	0.002449	-0.006592	0.5294	<0.0001
	association	0.000982	1.157	0.4563	0.0003
	orientation	-0.00288	5.991	0.2013	0.0054

1  
2  
3  
4  
5  
6  
7  
8  
9  
10  
11  
12  
13  
14  
15  
16  
17  
18  
19  
20  
21  
22  
23  
24  
25  
26  
27  
28  
29  
30  
31  
32  
33  
34  
35  
36  
37  
38  
39  
40  
41  
42  
43  
44  
45  
46  
47  
48  
49  
50  
51  
52  
53  
54  
55  
56  
57

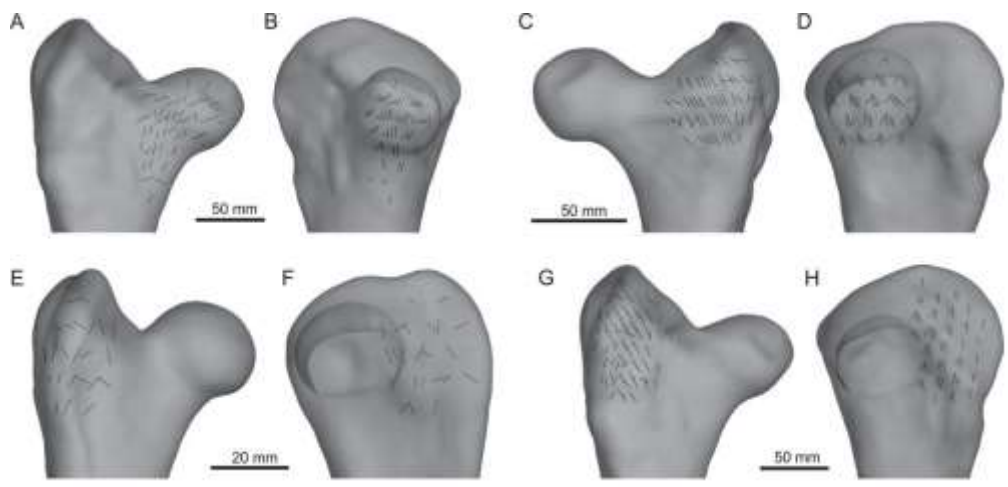


Figure 1

58  
59  
60

URL: <http://mc.manuscriptcentral.com/talc> E-mail: [steve.mcloughlin@nrm.se](mailto:steve.mcloughlin@nrm.se)

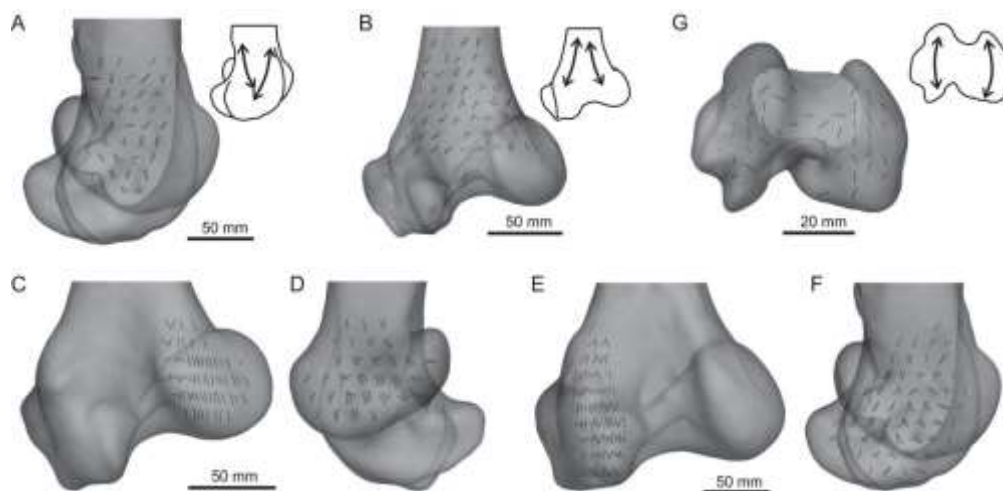


Figure 2

1  
2  
3  
4  
5  
6  
7  
8  
9  
10  
11  
12  
13  
14  
15  
16  
17  
18  
19  
20  
21  
22  
23  
24  
25  
26  
27  
28  
29  
30  
31  
32  
33  
34  
35  
36  
37  
38  
39  
40  
41  
42  
43  
44  
45  
46  
47  
48  
49  
50  
51  
52  
53  
54  
55  
56  
57  
58  
59

1  
2  
3  
4  
5  
6  
7  
8  
9  
10  
11  
12  
13  
14  
15  
16  
17  
18  
19  
20  
21  
22  
23  
24  
25  
26  
27  
28  
29  
30  
31  
32  
33  
34  
35  
36  
37  
38  
39  
40  
41  
42  
43  
44  
45  
46  
47  
48  
49  
50  
51  
52  
53  
54  
55  
56  
57  
58  
59  
60

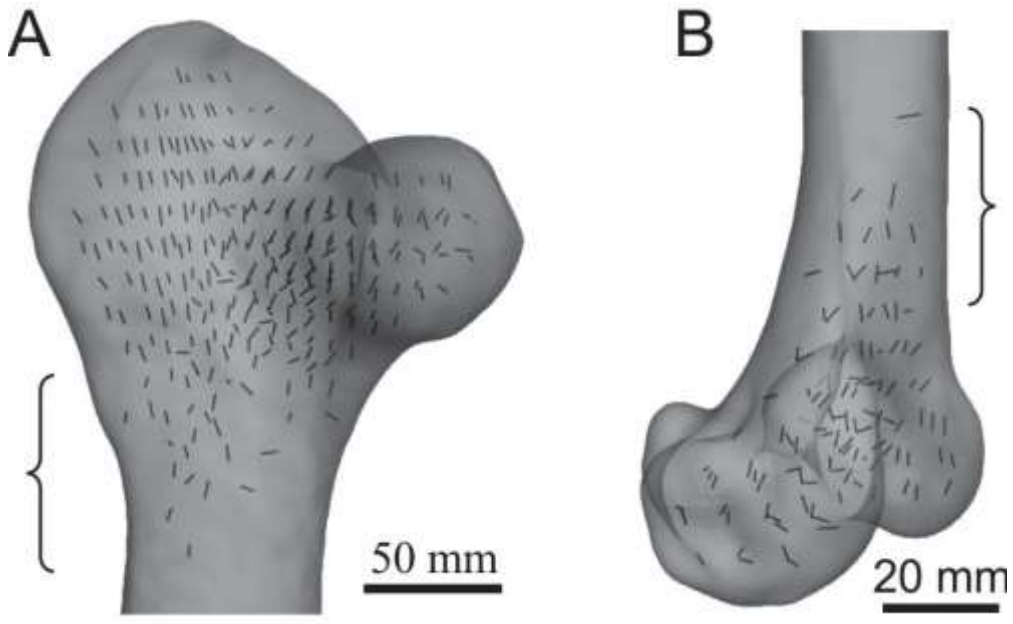


Figure 3

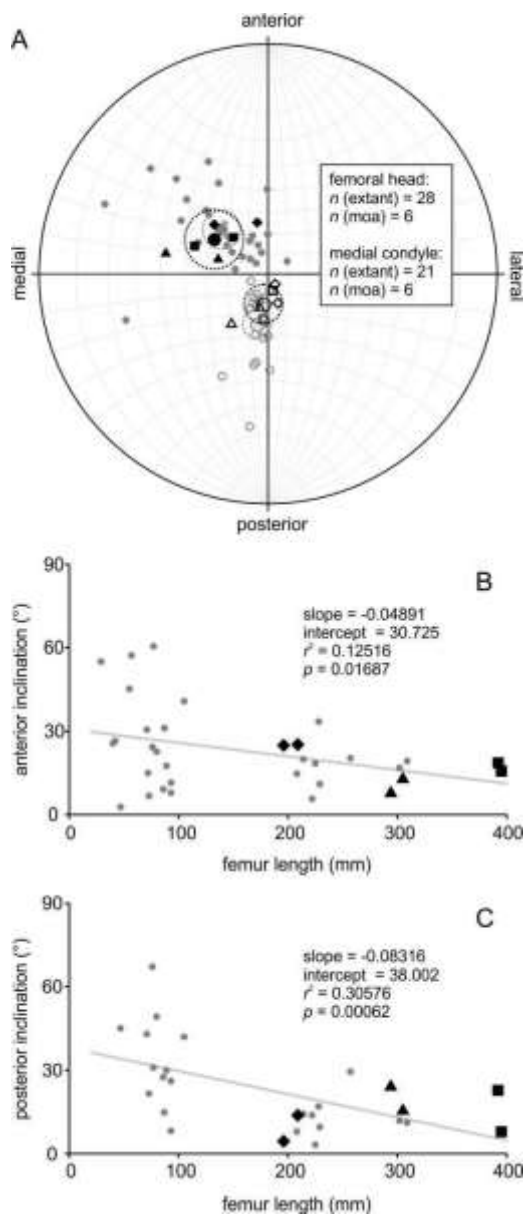


Figure 4

1  
2  
3  
4  
5  
6  
7  
8  
9  
10  
11  
12  
13  
14  
15  
16  
17  
18  
19  
20  
21  
22  
23  
24  
25  
26  
27  
28  
29  
30  
31  
32  
33  
34  
35  
36  
37  
38  
39  
40  
41  
42  
43  
44  
45  
46  
47  
48  
49  
50  
51  
52  
53  
54  
55  
56  
57  
58  
59  
60

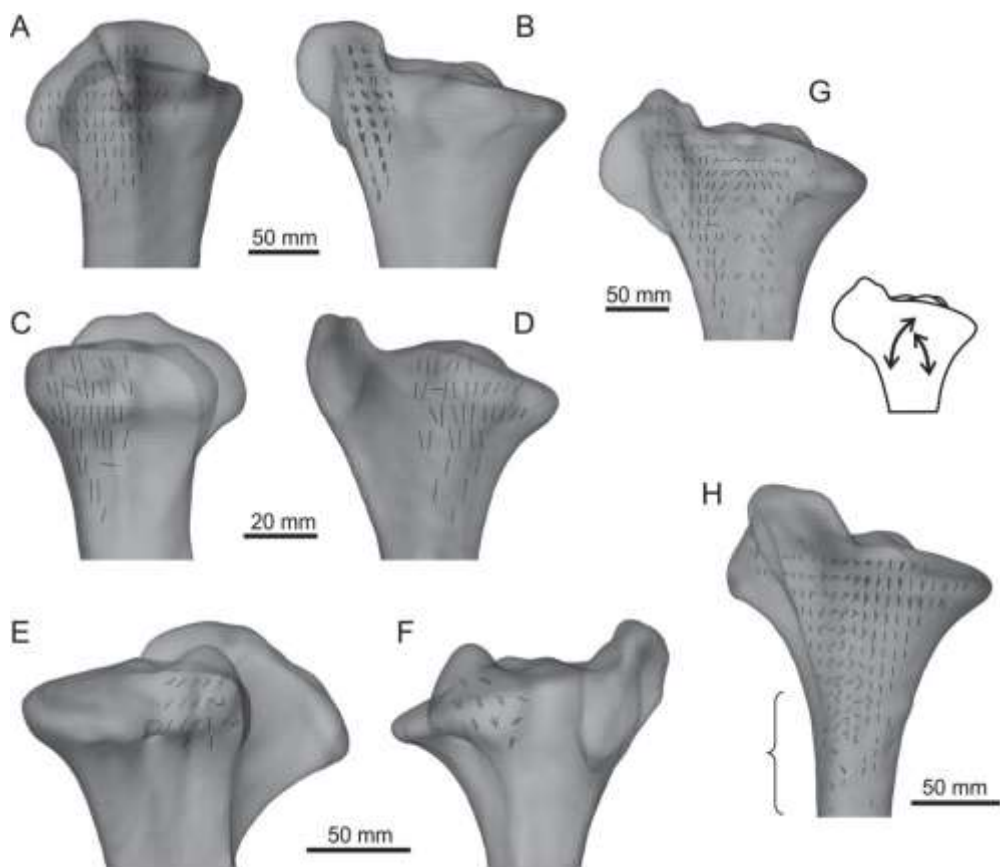


Figure 5

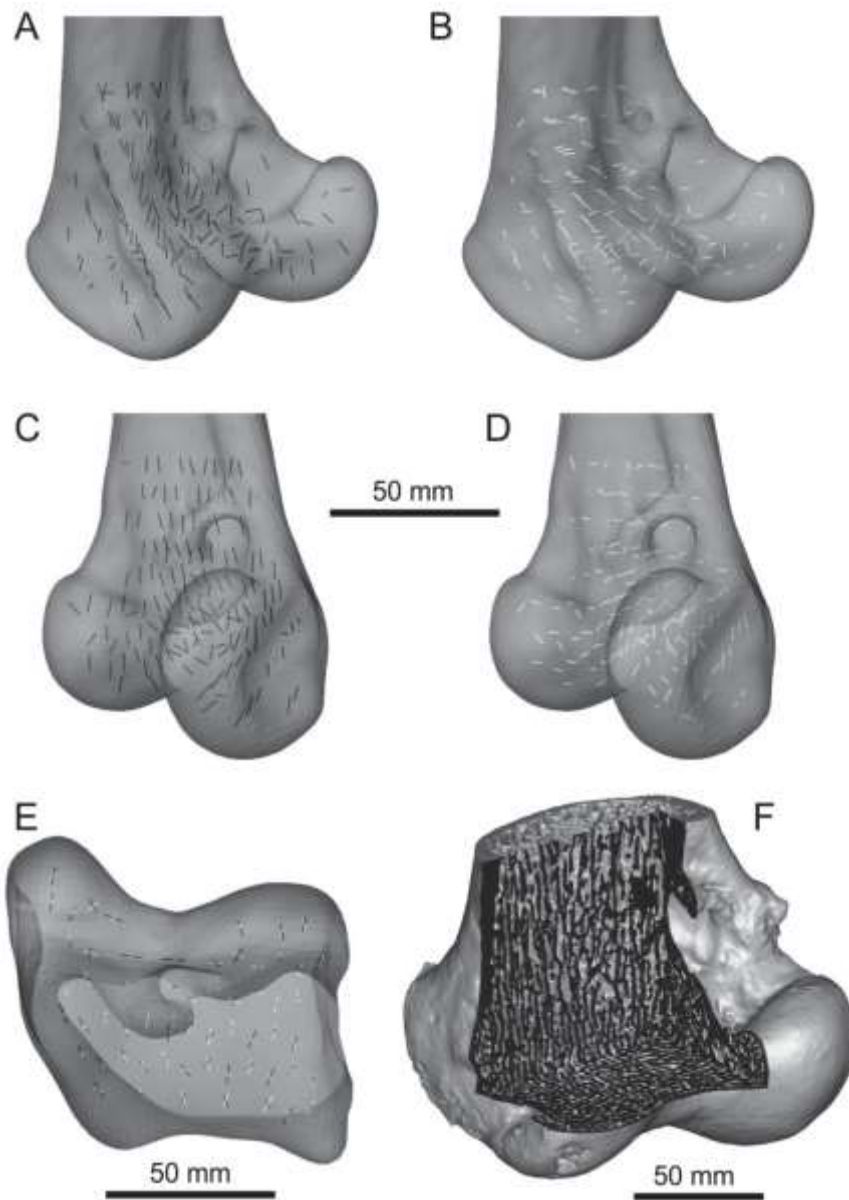


Figure 6

1  
2  
3  
4  
5  
6  
7  
8  
9  
10  
11  
12  
13  
14  
15  
16  
17  
18  
19  
20  
21  
22  
23  
24  
25  
26  
27  
28  
29  
30  
31  
32  
33  
34  
35  
36  
37  
38  
39  
40  
41  
42  
43  
44  
45  
46  
47  
48  
49  
50  
51  
52  
53  
54  
55  
56  
57  
58  
59  
60

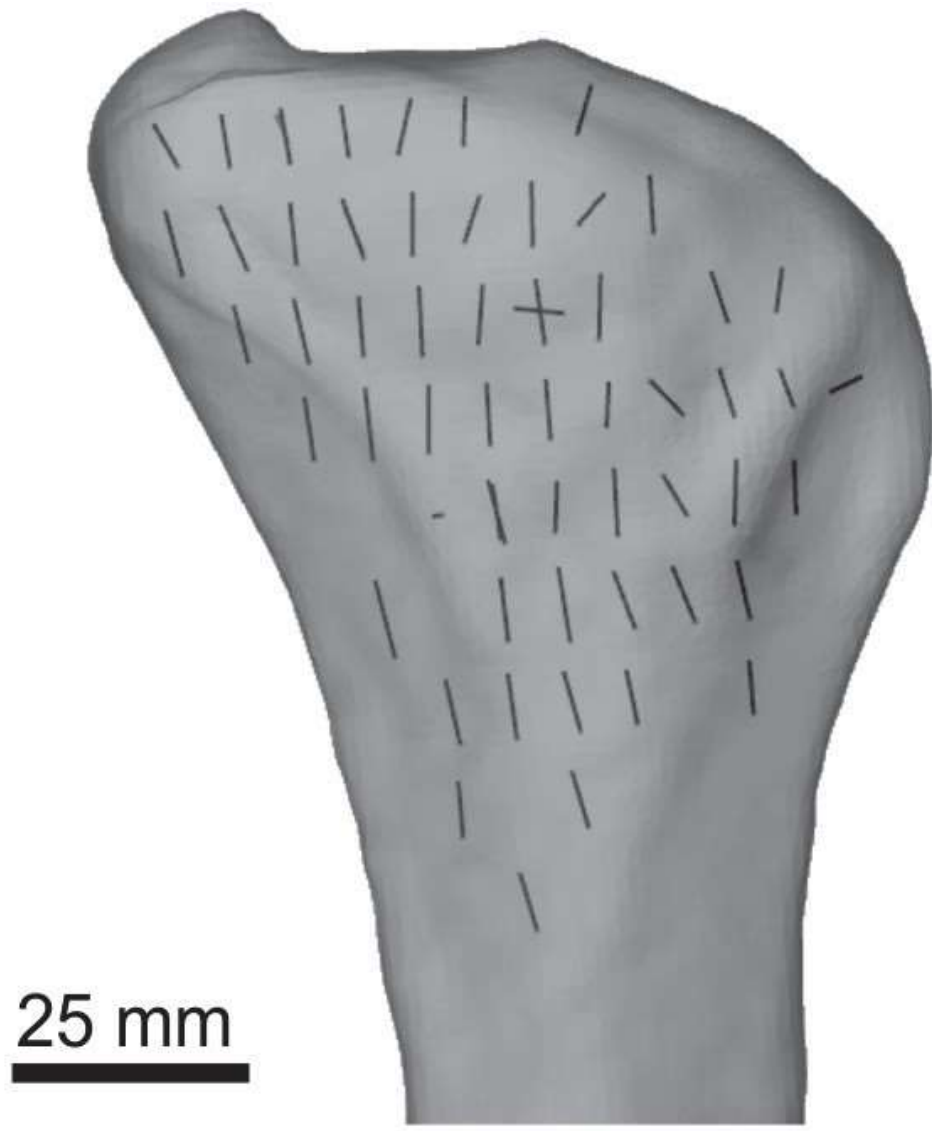


Figure 7

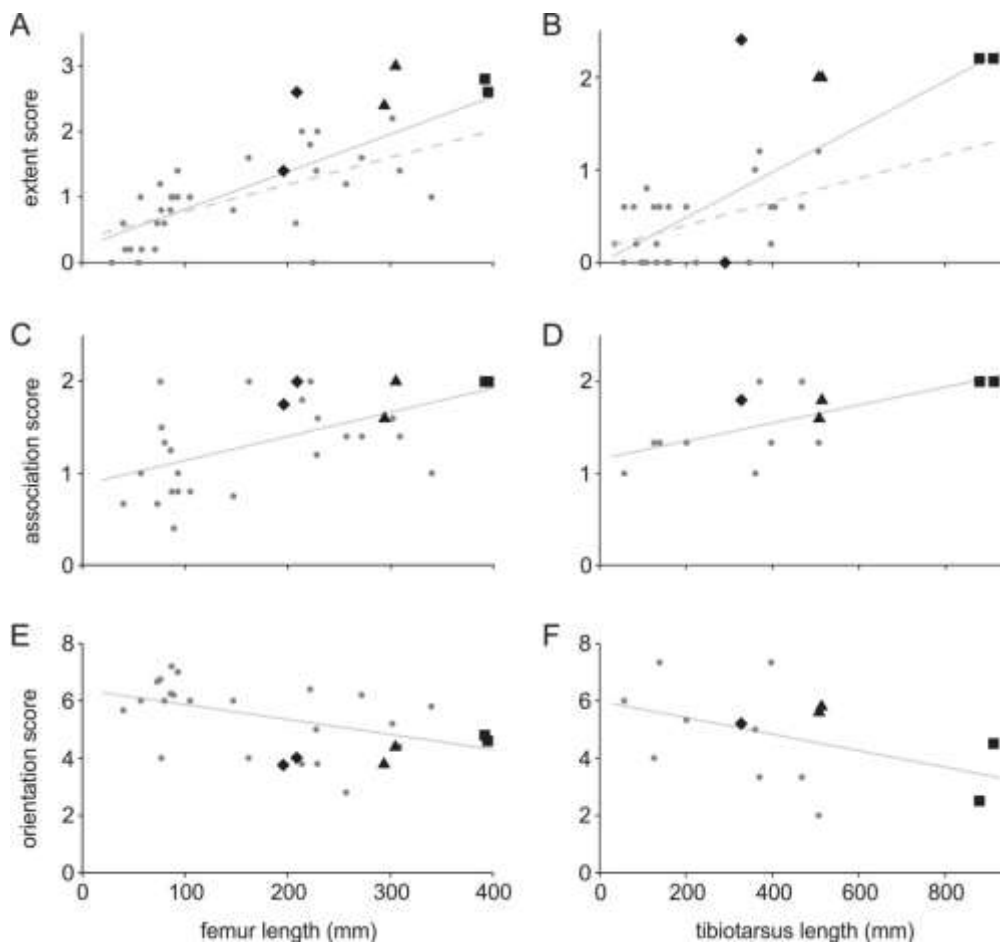


Figure 8

1  
2  
3  
4  
5  
6  
7  
8  
9  
10  
11  
12  
13  
14  
15  
16  
17  
18  
19  
20  
21  
22  
23  
24  
25  
26  
27  
28  
29  
30  
31  
32  
33  
34  
35  
36  
37  
38  
39  
40  
41  
42  
43  
44  
45  
46  
47  
48  
49  
50  
51  
52  
53  
54  
55  
56  
57  
58  
59  
60

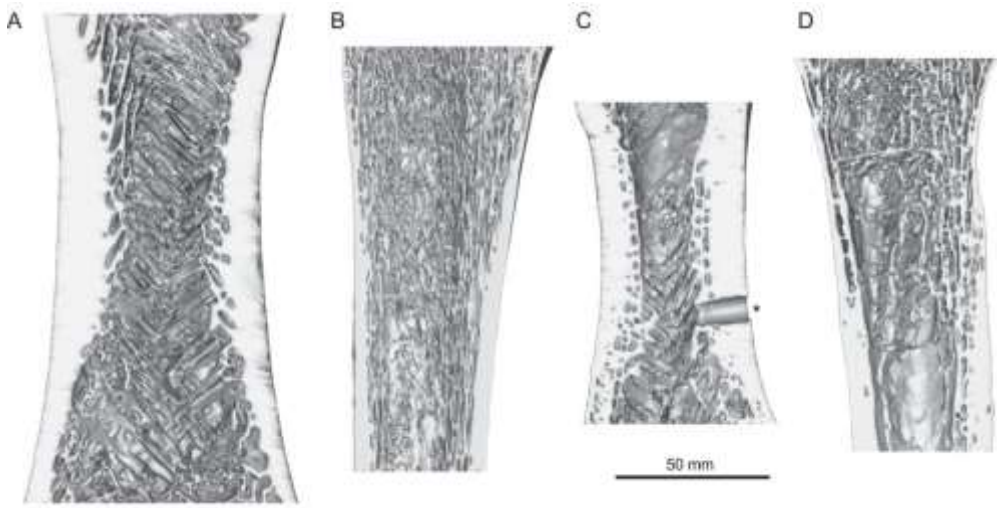


Figure 9